Loss of canonical sex steroid signaling correlates with prostate cancer progression and induces tumor escape in *Drosophila*

Authors: M. Vialat[1,2]†, E. Baabdaty[1,2]‡, C. Vachias[1,2], F. Degoul[1,2], A. Trousson[1,2], P. Pouchin[1], JMA. Lobaccaro[1,2], S. Baron[1,2], L. Morel[1,2], C. de Joussineau[1,2]*.

Affiliations:

[1]Université Clermont Auvergne, CNRS 6293, INSERM 1103, iGReD; Clermont–Ferrand, France.

[2] Groupe Cancer Clermont Auvergne; Clermont-Ferrand, France.

*Corresponding author. Email: cyrille.de_joussineau@uca.fr.

† Present address: Icahn School of Medicine at Mount Sinai, New York city, USA.

‡ Present address: Institut de la vision, Paris, France.

Abstract: In cancer, tumor escape often arises following treatments. This is especially true during deprivation therapies, where this phenomenon has been linked to steroid signaling reactivation despite deprivation. Here, we show that in prostate cancer tissues the canonical androgen pathway itself is deactivated and, in fact, loss of canonical AR signaling tightly correlates with cancer progression. This raises the possibility that loss of canonical sex steroid signaling could promote the progression. We tested this hypothesis a drosophila model of prostate cancer. There, repression of canonical sex steroid ecdysone receptor signaling displays both anti- and protumor effects. On the one hand, it slightly decreases extra-epithelial tumor formation, and increases their propensity for apoptosis. On the other hand, it induces

the growth of a new tumor cell population, which growth is normally prevented by autocrine/intracrine ecdysone signaling. Furthermore, this population appears to emerge from epithelial clones within the gland. To do so, tumor cells change the way they migrate out of the epithelium, forming a new layer between the normal epithelium and the basement membrane. This depends on a modification of epithelial basal extrusion that likely relies on the downregulation of Ecdysone target gene *βTub60D*. Thus, in drosophila accessory gland, lack of sex steroid signaling not only coincides with but actually induces tumor escape. Together, these results question the role of sex steroid deprivation on tumor progression, and point to altered basal extrusion as a possible mechanism shaping tumor escape.

Introduction

Epithelial tumorigenesis is a complex, multistep process spanning from hypothetical initiation to metastatic spread. Late stages are better characterized, and have been associated with numerous alterations in molecular mechanisms that appear necessary for tumor progression (reviewed in (Hanahan and Weinberg, 2011)). Among them, specific pathways can act in specific tissues. Typically, the main sex steroids, estrogens and androgens, support growth of adenocarcinoma in reproductive tissues. Accordingly, endocrine therapy (sex steroid deprivation) is widely used in breast and prostate cancers to induce tumor regression. However, despite strong initial response, tumor escape frequently occurs and even systematically in prostate cancer. Tumor escape is frequently associated with resistance to hormone deprivation. Treatment-resistant cells can adapt through high estrogen or androgen receptor (ER or AR) expression enabling sensitivity to reduced steroid levels, ER/AR mutations or alternative splicing leading to ligand-independent reactivation (Cao et al., 2014; Zundelevich et al., 2020). However, tumor escape also occurs when tumor cells become completely independent of steroid signaling for their progression, following *ER*/*AR* loss of function (Kuukasjärvi et al., 1996). So, it exists more than one path for tumor cells to survive endocrine therapy. Furthermore, cells that escape treatment appear more aggressive, with higher proliferative and metastatic potential (Clarke et al., 1989; Wu et al., 1994).

Despite best efforts, the origin of the cells that escape endocrine therapy remains debated, and the mechanisms allowing them to develop into tumors are still largely unknown. Over the last decades, cancer stem cells (CSCs) have emerged as strong candidates for initiating resistant tumor growth (Rodriguez et al., 2019; Rybak et al., 2015). Detected in many tumor types, these cells are defined by their insensitivity to treatments and their ability to recolonize a tumor that regresses upon treatment (Atashzar et al., 2020). Why these cells are present remains under scrutiny: hypothetically, they could already be present before treatment as a

consequence of stochastic tumor heterogeneity, derive from adult stem cells, or transdifferentiate from tumor cells as a consequence of treatment selection. This last hypothesis, implying that deprivation therapy would in part be responsible for tumor progression, is supported by the observation that xenografted tumor cells can escape androgen deprivation in castrated mice (Iwasa et al., 2007; Nagabhushan et al., 1996; Wu et al., 1994; Zhou et al., 2004). However, the cellular and molecular mechanisms by which these cells could emerge and regrow to form a tumor are mostly unknown.

We previously developed a model of epithelial tumorigenesis in the drosophila accessory gland (Rambur et al., 2020). Thanks to its versatility as a genetic model, drosophila has been successfully used in cancer biology to decipher fundamental mechanisms in brain cancer development (Read, 2011; Read et al., 2009) as well as epithelial cancers such as lung (Levine and Cagan, 2016) and colon cancers (Bangi et al., 2016). It has even recently been used as a platform for precision medicine in cancer therapy, demonstrating its direct relevance to patient care (Bangi et al., 2019). Most prostate adenocarcinomas are thought to originate from luminal cells (Humphrey, 2012). The drosophila accessory gland is a functional equivalent of the prostate (Leiblich et al., 2012; Wilson et al., 2017; Xue and Noll, 2002) mainly composed of a monolayer of seminal fluid-secreting cells (Taniguchi et al., 2018; Xue and Noll, 2002) surrounded by a monolayer of stroma-like muscle cells encased in a strong basement membrane (Rambur et al., 2020). It is an established model to study mechanisms of epithelial prostate tumorigenesis (Ito et al., 2014; Molano-Fernández et al., 2022; Rambur et al., 2021, 2020; Vialat et al., 2024; Wilson et al., 2017). Furthermore, accessory gland differentiation and activity are driven by the drosophila sex steroid Ecdysone Receptor (EcR) (Sekar et al., 2023; Sharma et al., 2017), paralleling the role of human Androgen Receptor (AR) in the prostate physiology.

81 In this study, we have first interrogated prostate cancer patient expression data. We find that
82 in Castration Resistant Prostate Cancer (CRPC), there is no evidence of canonical AR
83 signaling reactivation; in fact, canonical AR signaling is significantly repressed in CRPC
84 compared to primary tumors. Furthermore, cancer progression tightly correlates with this loss
85 of canonical AR signaling. These data raise the possibility that this loss could participate to
86 tumor resistance. However, due to the existence of non-canonical pathways, of multiple
87 escape mechanisms and of frequent crosstalk with other steroid signaling such as
88 Glucocorticoid Receptor, which in resistance expresses AR target genes (Arora et al., 2013),
89 it appears difficult to study the specific effect of sex steroid canonical pathway repression on
90 cancer progression. To study this effect, we turned to drosophila where only one steroid is
91 known, ecdysone. So, we reproduced endocrine therapy in the drosophila accessory gland by
92 genetically inducing tumor-specific ecdysone signaling downregulation. We show that
93 repression of canonical sex steroid signaling actively reprograms pre-existent tumor cells to
94 create a new tumor cell population that escapes this sex steroid deprivation. This deprivation
95 induces a newly uncovered kind of basal extrusion, *de facto* creating a new niche for tumor
96 development in what we define as the intrabasal compartment. This change notably relies on
97 downregulation of EcR target gene *βTub60D*, which encodes β3 Tubulin (β3Tub).
98 These findings possibly shed new light on the mechanisms of tumor escape.

99 # Results

100 ## Canonical Androgen signaling decreases with cancer progression

101 ### *Canonical Androgen signaling genes are downregulated in CRPC compared with primary*
102 ### *cancer*

103 Even though it is commonly accepted that CRPC corresponds to a phase of reactivation of AR
104 signaling, we first assessed how much activity of canonical androgen signaling can be

105 detected depending on the stage of prostate cancer. Because AR is a transcription factor,
106 transcription of target genes was used as a readout across more than 1000 tumor samples from
107 several public datasets (Abida et al., 2019; Beltran et al., 2016; Cancer Genome Atlas
108 Research Network et al., 2015; Kumar et al., 2016; Labrecque et al., 2019; Lapuk et al., 2012;
109 Sharp et al., 2019; Stelloo et al., 2018; Suntsova et al., 2019; "The Genotype-Tissue
110 Expression (GTEx) project.," 2013) and grouped in the Prostate Cancer Atlas
111 (prostatecanceratlas.org). This tool was initially introduced by Bolis et al (Bolis et al., 2021).
112 We first observed that *AR* expression significantly increases in primary prostate cancer
113 compared to normal tissue, and increases again in CRPC samples compared to primary cancer
114 (Fig. 1A). We then explored the androgen response using expression of several target genes of
115 AR signaling (*ABCC4*, *ALDH1A3*, *AMACR*, *CAMK2*, *FASN*, *KLK2*, *KLK3*, *NKX3-1*, *PART1*,
116 *PCA3*, *PLPP1*, *PMEPA1*, *STEAP1*, *STEAP2*, *STEAP4*). All these genes exhibit the same
117 expression profile. Compared to normal samples, they are all significantly overexpressed in
118 primary samples, as is *AR*. However, in CRPC samples and even though *AR* expression is still
119 increased there, they are all significantly repressed compared to primary samples (Fig. 1B,
120 Table 1). In fact, six of these genes (*ABCCC4*, *ALDH1A3*, *KLK2*, *KLK3*, *PART1*, *STEAP4*)
121 are expressed at even lower levels in CRPC than in normal tissues (Fig. 1B,Table 1).

122 ***Canonical Androgen signaling gene expression negatively correlates with prostate cancer***
123 ***progression***

124 The Prostate Cancer Atlas also correlates changes in transcriptomic profiles with cancer
125 progression (i.e. pseudotime progression, Fig.1C), with a high degree of confidence, allowing
126 retrospective association of specific changes in gene expression with the cancer trajectory.
127 Logically, plotting individual patients on this trajectory discriminates normal tissue (green,
128 low pseudotime, Median ± Std error = 54.58 ± 2.396), primary cancer (red, intermediate
129 pseudotime = 105.9 ± 0.7952) and CRPC (blue, high pseudotime = 196.5 ± 1.322) among

130 which the most aggressive form -neuroendocrine cancers (NEPC, violet)- clusters at the final
131 tip of the trajectory (Fig. 1D). *AR* expression itself peaks in CRPC samples (Fig. 1E) but only
132 weakly correlates with progression (Fig.1F, R = 0.11, FDR = 0.0459). To understand why this
133 correlation is so weak, we plotted *AR* expression against pseudotime (Fig. 1G). *AR* expression
134 there appears to vary widely in CRPC samples. We therefore subdivided CRPC samples into
135 four groups based on pseudotime, i.e., their state of progression (Fig. 1H). The 1st quartile
136 (1ST QT) displays mean AR expression of 11.41 ± 0.16; 2ND QT is significantly lower at
137 10.83 ± 0.15 (p = 0.0209). Decrease from quartile to quartile continues for 3RD QT (8.82 ±
138 0.22, p<0.0001) and 4TH QT (5.27 ± 0.31, p<0.0001). Thus, even though *AR* expression
139 clearly increases in primary cancer and then CRPC, its expression steadily decreases within
140 CRPC when state of progression is considered.

141 At the same time, canonical androgen signaling appears as the most downregulated pathway
142 along cancer progression -especially in CRPC samples (Bolis et al., 2021)- as shown for
143 *SPOP*, one of the most frequently mutated genes in prostate cancer and a key player in
144 genome integrity (Barbieri et al., 2012; Boysen et al., 2015) (Fig. 1I-J, R = -0.64, p = 1.93e-
145 52), *KLK3* -coding for the Prostate Specific Antigen (Fig. 1K-L, R = -0.63, p = 7.72e-64)- or
146 *NKX3-1,* which is itself a specific prostate tumor suppressor gene (Bhatia-Gaur et al., 1999)
147 (Fig. 1M-N, R = -0.60, p = 1.79e-54). Overall, even though *AR* itself is globally more
148 expressed in CRPC patients, canonical androgen signaling definitely decreases with cancer
149 progression.

150 ***CRPC-specific loss of correlation between AR expression and canonical AR signaling***

151 To understand this phenomenon, we plotted expression of *AR* expression against its target
152 genes (here *ALDH1A3*) for normal, primary cancer or CRPC samples (Fig. 2A). In normal
153 tissues, *AR* and *ALDH1A3* expression are concentrated in a relatively narrow range, making
154 all samples look alike (Fig. 2B). In primary cancer, the increase in *AR* expression (from 6.93

155 ± 0.81 to 7.42 ± 0.64, p<0.0001) correlates with an increase in *ALDH1A3* expression (from
156 7.67 ± 1 to 9.07 ± 0.97, p<0.0001), keeping samples close to each other but shifted to a higher
157 expression range compared to normal samples (Fig. 2C). However, in CRPC samples, despite
158 a still higher *AR* median expression (from 7.42 ± 0.64 to 9.93 ± 3.37, p<0.0001), individual
159 *AR* expression is dispersed over more than 10 logs (from 0.11 to 13.16). *ALDH1A3*
160 expression also varies hugely across samples, but with a Pearson Coefficient of 0.494,
161 remains weakly correlated with AR expression in individual samples. However, *ALDH1A3*
162 expression does strongly decrease (from 9.07 ± 0.97 to 5.83 ± 1.97, p<0.0001) in CRPC (Fig.
163 2D), indicating that AR does not appear to activate expression of this gene as efficiently as in
164 normal or primary cancer tissues.

165 We then wondered whether androgen metabolism itself could be disturbed. Interestingly,
166 *SRD5A2*, which encodes the enzyme responsible for the production of the active metabolite of
167 testosterone, DiHydroTestosterone (DHT) (Andersson et al., 1991), is downregulated in
168 primary samples and even more so in CRPC samples (Fig. 2E). *SRD5A2* is in fact one the
169 most downregulated genes during cancer progression (Fig. 2F, Fig. 2G, R=-0,82, p=1.23e-
170 143). However, its progressive loss of expression starts from primary cancer (Fig. 2H).
171 Potentially, the lack of response to the peak of AR expression in early CRPC could result
172 from reduced DHT metabolization that begins in primary tumors. Indeed, DHT levels are
173 lower in untreated cancer tissues than in benign prostatic hyperplasia (Geller et al., 1978).
174 Furthermore, in men suspected of prostate cancer who underwent needle biopsies, a high
175 percentage of cancer-positive cores -associated with poor prognosis- also correlates with
176 lower DHT levels (Miyoshi et al., 2014). Thus, DHT concentration decreases in prostate
177 cancer even before castration and castration resistance, and correlates with poor prognosis.
178 Overall, transcript analysis of major prostate cancer cohorts indicates that canonical Androgen

179 Receptor signaling negatively correlates with cancer progression, even in samples classified
180 as hormone refractory in which androgen signaling is generally considered active.

181 **Tumor escape induced by Ecdysone Receptor downregulation**

182 Considering these results, we asked whether repression of canonical sex steroid signaling
183 could by itself induce cancer progression. To test this hypothesis, we turned to a drosophila
184 model of prostate cancer we previously engineered, in which we can also study in detail the
185 phenomenon of basal extrusion, considered as the founding step of cancer formation.

186 ***Epithelial tumor cells and extra-epithelial tumors in EGFRλ-mediated tumorigenesis***

187 Thanks to genetic tools available in drosophila based on the UAS/Gal4 expression system, it
188 is possible to reproduce tumor initiation in the drosophila accessory gland. For this, clonal
189 expression of a constitutively active form of EGFR -EGFRλ- is realized in ~1% of the main
190 cells of the accessory gland. This oncogene is co-expressed with GFP, allowing tracing of
191 tumor cells. To provide an adequate control for tumorigenesis (EGFRλ CTL), it is
192 furthermore co-expressed with a second nuclear GFP, as every condition must bear the same
193 number of UAS elements to avoid Gal4 titration effect. Under these conditions, tumor
194 initiation displays different outcomes. Some clonal cells undergo proliferation at low rates but
195 do not migrate, and thus remain inside the epithelium (Fig. S1A-F, *i.e.* clones, white
196 arrowheads). Among these cells, some display disorganized cell-cell interaction markers,
197 indicating disturbed epithelial differentiation and probable loss of adhesion with neighbor
198 cells (Fig. S1A-C, thick empty arrowheads). Due to their mild hyperproliferation, these cells
199 can be considered part of benign tumors. Finally, some clonal cells migrate and develop into
200 extra-epithelial tumors (Fig. S1D-F, empty arrowheads), where cells are completely devoid of
201 epithelial markers (Fig. S1F), indicating in drosophila a phenomenon of Epithelial-
202 Mesenchymal Transition (EMT).

203 As demonstrated by their presence outside the muscle sheet that encloses the gland (revealed
204 by F-actin staining in Fig. 3A and later), these tumor cells invade through the basement
205 membrane, a behavior known as epithelial basal extrusion that is specific to cancer cells
206 according to the National Cancer Institute. We previously showed that these extra-epithelial
207 tumors harbor phenotypic abnormalities typically associated with tumor development, such as
208 hyperplasia, hypertrophy, loss of epithelial marker expression (Fig. S1F, Fig. 3) and
209 promotion of angiogenesis-like tracheogenesis. We also previously described that many of
210 them retain a specific feature of accessory gland epithelial cells -twin nuclei- confirming that
211 these cells originate from the accessory gland (Rambur et al., 2020).

212 ***Treatment-like effect induced by Ecdysone Receptor downregulation***

213 We further evaluated *EcR* expression during tumorigenesis. By RNA FISH, we show that *EcR*
214 is overexpressed in tumor cells that were able to extrude basally (Fig. 3A-B). This
215 phenocopies *AR* overexpression in human prostate cancer and raises questions about the
216 potential role of EcR in accessory gland tumorigenesis. We so co-expressed an RNAi
217 targeting EcR with the oncogene (EGFRλ EcR-KD, Fig. 3C-D). At first sight, this co-
218 expression induces growth of epithelial clones and extra-epithelial tumors similar to the
219 control (compare white and empty arrowheads in Fig. 3E-H to Fig. 3I-L). At 6D,
220 tridimensional reconstruction of image stacks indicates that the tumors display the same
221 volume and the same number of cells in both conditions (Fig. 3M, N). Thus, these tumors
222 display similar proliferation rate of ~700% compared with clones expressing GFP only (Fig.
223 3O), which are typically composed of two cells at six days of induction (Fig. S3A). We
224 conclude that phenotypic development of extra-epithelial tumors does not rely on ecdysone
225 signaling. We then examined whether extra-epithelial tumor formation itself is modified.
226 Temporal dynamics of extra-epithelial tumor formation is not affected by EcR RNAi co-
227 expression (Fig. 3P): extra-epithelial tumors typically start to appear between the third and

228 fourth days after clonal induction (3D and 4D), peaking at 5D regardless of genotype,
229 indicating that basal extrusion is active only during this short period of time. However, a
230 modest but significant decrease in the total number of extra-epithelial tumors is detected upon
231 EcR downregulation (Fig. 3Q). Together, these data show that loss of ecdysone signaling
232 specifically affects the overall quantity of tumor basal extrusion, but has neither an effect on
233 its temporal dynamics nor on tumor growth rate outside the gland.

234 In human, sex steroid deprivation also induces death of treatment-sensitive tumor cells
235 (Dowsett et al., 2006; Isaacs et al., 1994). 6 days after clone induction (6D), cleaved-caspase
236 3 staining reveals that, in the control condition, tumor cells do not present signs of apoptosis
237 (Fig. 3R-S). However, at the same time point, EcR RNAi co-expression significantly induces
238 apoptosis in extra-epithelial tumors (Fig. 3T-U, empty arrowheads in left panels; middle
239 columns in Fig. 3V for quantification). This indicates that, in the drosophila accessory gland,
240 some tumor cells rely on sex steroid signaling for their survival, as in the human disease.

241 Interestingly, at 10 days after induction (10D), most extra-epithelial tumors harbor apoptotic
242 staining, independently of genotype (Fig. 3V, right columns). Thus, despite their ability to
243 undergo the complex program of basal extrusion, these cells seem unable to survive for long
244 periods, indicating limited tumor potential.
245 Together, these results indicate that repression of EcR in accessory gland tumors cells
246 displays a treatment-like effect: extra-epithelial tumor formation is (slightly but) significantly
247 impaired, and cells composing these tumors are sensitive to this deprivation and undergo
248 apoptosis.

249 ***Tumor escape induced by Ecdysone Receptor downregulation***

250 Strikingly, in EGFRλ EcR-KD condition, we also detect a new type of tumorigenesis: large
251 tumor masses now grow inside the glands (Fig. 3T, Fig. 4A-D, yellow arrowheads). Thus,

252 generation of this new phenotype apparently depends solely on lack of ecdysone signaling in
253 tumor cells. Contrary to the cells that remain in the epithelium in the EGFRλ CTL condition,
254 these cells generally express low levels of epithelial markers (Fig. 4D), indicating a loss of
255 epithelial differentiation. Notably, unlike extra-epithelial tumors, this new tumor cell
256 population shows no sign of apoptosis regardless of induction time (Fig. 4E-H), and tend to
257 invade the whole gland, unlike clone cells in the EGFRλ CTL condition (white arrowheads in
258 Fig. 4E-F, yellow arrowheads in Fig. 4G-H). Thus, this new population displays an increased
259 proliferative capacity compared with the EGFRλ CTL condition. Together, this indicates that
260 these cells are not only escaping EcR repression but also now thrive over time under this
261 stress.

262 ***Markers of higher progression of the new tumor cell population***

263 Contrary to tumor cells in EGFRλ CTL condition, this new cell population displays strong
264 staining for Ser10 Phospho-Histone 3 (pH3), a marker of late phases of the cell cycle prior to
265 cell division (compare white to yellow arrowheads in Fig. 4G-H to 4I-J). Furthermore, they
266 exhibit a positive staining for phosphorylated proto-oncogene tyrosine-protein kinase Src
267 (pSrc), a classical marker of aggressiveness (compare white to yellow arrowheads in Fig. 4K-
268 L to 4M-N) (Baumgartner et al., 2008). These tumor cells also display many typical defects,
269 such as a clear pleomorphism with either compact or fusiform cells, and strongly disorganized
270 clones (Fig. 4Q-T). In the same clone and even within the same cell, nuclei differ markedly in
271 size (anisocaryosis) with frequent hypertrophied nuclei (macrocaryosis). Nuclei shapes are
272 often altered (empty arrowheads in Fig. 4Q-R). Clones can grow along multiple axes (double-
273 headed arrowheads in Fig. 4S-T) and present a strong fibrillar framework (Fig. 4T). Together,
274 these results highlight that this new population has reached a higher step of tumor progression
275 compared to previously described clones and extra-epithelial tumors, which form rounder,
276 well-delimited masses.

277 **Basal extrusion is modified in case of tumor escape**

278 We then asked how these new tumor cells appear inside the glands.

279 ***A second kind of basal extrusion unveiled by EcR downregulation***

280 In EGFRλ CTL condition (Fig. 5A-D, white arrowheads), as in case of co-repression of
281 Ras/MAPK, PI3K/Akt (Rambur et al., 2020) or cholesterol metabolic pathway (Vialat et al.,
282 2024), tumor clones that appear in the gland remain strictly in the epithelium (orthogonal
283 view in Fig. 5C-D, where phalloidin staining (yellow) indicates the position of the muscle
284 layer within the basement membrane). By contrast, in EGFRλ EcR-KD condition, the new
285 population of tumor cells grows between the normal epithelium (delineated by white dashes
286 in the orthogonal views in Fig. 5G-H) and the basement membrane (Fig. 5E-H, yellow
287 arrowheads). Thus, these cells were able to migrate basally out of the normal epithelium,
288 thereby pushing it into the gland lumen. At the same time, they did not cross the basement
289 membrane. This redefines basal extrusion as two different phenomena with a common start.
290 In this first step, cells extrude basally from the epithelium. Then, cells can either cross the
291 basement membrane and form extra-epithelial tumors or, depending on *EcR* repression, grow
292 inside the gland. Blocking ecdysone signaling therefore promotes a new tumor cell fate, in
293 which tumor cells accumulate between the normal epithelium and the basement membrane,
294 forming highly proliferative tumors that escape steroid signaling downregulation in what we
295 define as the intrabasal (IB) compartment.

296 ***Intrabasal growth relies on a new, inducible kind of basal extrusion***

297 Given that we concomitantly detected a slight decrease in extra-epithelial tumor formation in
298 the EGFRλ EcR-KD condition (Fig. 3Q), we asked whether formation of intrabasal tumors
299 arises from a redirection from full basal extrusion to partial basal extrusion. We show that, in
300 contrast to extra-epithelial tumors, intrabasal tumors continue to appear and grow over time,

301 as more glands display at least one intrabasal tumor at 7D than at 6D (Fig. 5I); thus, they
302 apparently do not replace lost extra-epithelial tumors. As a result of this growth, at 7D there
303 are already significantly more glands displaying an intrabasal tumor that the maximal
304 percentage of extra-epithelial tumors achieved in the EGFRλ CTL genotype (61.6% vs
305 49.6%, $p<0.001$. N=29, n=1117 vs N=3, n=268). This shows that, in EGFRλ EcR-KD
306 condition, formation of intrabasal tumors does not result from mere inhibition of full basal
307 extrusion but from promotion of a different kind of basal extrusion that ultimately generates
308 tumor escape.

309 We then characterized these intrabasal tumors. At 6D, intrabasal tumors (IB-T) are
310 significantly smaller than extra-epithelial tumors (T) but still significantly larger than
311 epithelial clones of EGFRλ CTL genotype (C) (Fig. 5J). This increase in volume mostly
312 results from an increased proliferation rate and, consequently, increased tumor cell number in
313 intrabasal tumors, which at 6D already compares with that of extra-epithelial tumors (Fig. 5K-
314 L). Thus, considering the total percentages of extra-epithelial and intrabasal tumors, *EcR*
315 downregulation more than doubled the number of tumor cells during the course of the
316 experiment.

317 Overall, *EcR* knockdown in tumor cells displays two opposite effects. On the one hand, it
318 induces apoptosis of extra-epithelial tumors and modestly decreases their rate of formation.
319 On the other hand, it strongly induces a new kind of tumorigenesis, which develops and
320 thrives in the newly uncovered intrabasal compartment.

321 **Ecdysone-dependent molecular control of tumor escape and basal extrusion**

322 We then sought to determine the molecular mechanisms linking EcR Signaling to
323 tumorigenesis. Prostate tumor escape is generally linked to resistance to androgen deprivation
324 where AR is able to be activated despite hormone deprivation, through activating mutations in

325 the gene or ectopic sex steroid production by tumors or their surrounding tissues. However,
326 patients data indicate a decreased canonical androgen signaling in CRPC (Fig. 1-2). It is
327 therefore important to understand whether the observed escape results from a mechanism of
328 resistance or from a genuine lack of ecdysone signaling. We therefore downregulated multiple
329 targets at different levels of this pathway in a normal or tumoral context (Fig. S2).

330 ***Loss of ecdysone signaling does not promote tumorigenesis by itself***

331 First, we tested the effect of a loss of ecdysone signaling in a non-tumoral context. As
332 previously shown (Rambur et al., 2020), at 6D, clones expressing GFP are composed of two
333 cells (Fig. S3A). Downregulation of EcR expression (EcR RNAi) or impairment of ecdysone
334 synthesis (Shadow RNAi, Sad-KD, see Fig. S2) induces the same effect: as in CTL, clones
335 are composed of two cells that appear of normal shape and nuclear number (Compare Fig.
336 S3A and S1B and S3C). No tumorigenesis is detected (Fig. S3D). The only detected
337 phenotype is a slight decrease in epithelial cell growth without change in proliferation (Fig.
338 S3E-G). This hypotrophy could reflect a partial loss of cells' ability to produce seminal fluid,
339 which relies on ecdysone signaling in accessory gland cells.

340 ***Lack of canonical ecdysone signaling drives tumor escape***

341 Paralleling human metabolization of testosterone into active DiHydroTestosterone (DHT) by
342 the SRD5A2 gene product, ecdysone must be metabolized into active 20-hydroxyecdysone by
343 Shade (Shd) (Petryk et al., 2003). As *SRD5A2* dramatically decreases during cancer
344 progression (Fig. 2E-H), we downregulated *Shd* in tumor cells. Tumor progression is
345 phenocopied in glands of the EGFRλ Shd-KD genotype compared with the EGFRλ EcR-KD
346 condition, for both the decrease in extra-epithelial tumors and the growth of intrabasal tumors
347 (Fig. 6A, magenta columns). By targeting an independent gene, this confirms that lack of EcR
348 signaling leads to tumor resistance in the drosophila accessory gland.

349 Furthermore, ecdysone signaling relies on recruitment of specific EcR target genes -the early-
350 late transcription factors Hr3 and Hr4- to drive ecdysone responses (Carney et al., 1997;
351 Gauhar et al., 2009). Again, tumor progression in both EGFRλ Hr3-KD and EGFRλ Hr4-KD
352 conditions is strikingly similar to the EGFRλ EcR-KD condition (Fig. 6A-B, blue columns,
353 Fig. 6C-C', Fig. S3), showing that lack of canonical ecdysone signaling leads to tumor escape.

354 ***Complete dependence on tumor-produced Ecdysone to alleviate tumor escape***

355 Prostate cancer cells are able to produce steroids (Locke et al., 2008), which contribute to AR
356 reactivation in castration-resistant prostate cancer (CRPC) (Cai et al., 2011). In drosophila,
357 the Halloween genes encode the enzymes that synthetize ecdysone. Phantom (Phm) is the
358 limiting enzyme for this synthesis, whereas Shadow (Sad) is the terminal enzyme producing
359 ecdysone. The EGFRλ Phm-KD and EGFRλ Sad-KD conditions again phenocopy the
360 EGFRλ EcR-KD condition (Fig. 6A-B, red columns, Fig. 6D-D', Fig. S4). This shows -by
361 targeting still two other independent genes and still another process- that, in the drosophila
362 accessory gland, growth of intrabasal tumors results from lack of ecdysone signaling.
363 Furthermore, this demonstrates that circulating ecdysone cannot compensate for lack of
364 tumor-produced ecdysone, which is therefore the only indispensable resource to prevent
365 tumor escape in the accessory gland. We previously demonstrated that autocrine loops
366 recruiting Ras/MAPK and PI3K/Akt pathways are established to support basal extrusion
367 (Rambur et al., 2020). We show here that an autocrine/intracrine loop is also established to
368 activate ecdysone signaling and sustain the same phenomenon. However, blocking this loop
369 now also induces growth of intrabasal tumors, in contrast to inhibition of Ras/MAPK and
370 PI3K/Akt pathways. Thus, promotion of this mechanism of tumor escape is specifically
371 induced by the loss of ecdysone signaling in these cells.

372 ***EcR target gene Tub60D specifically represses intrabasal growth***

373 We then investigated molecular drivers that could promote intrabasal growth. Cytoskeletal
374 reorganization is a major determinant of tumor cell invasion and resistance, and intrabasal
375 tumor cells harbor profound cytoskeletal change. *Beta Tubulin at 60D* (*Tub60D*) encodes β3
376 Tubulin and is a target of ecdysone signaling (Bruhat et al., 1990). β3 Tubulin accumulates in
377 intra-epithelial clones of EGFRλ CTL condition but is mostly absent in intrabasal tumor cells
378 (compare Fig. 6E-F to G-H). Strikingly, downregulation of *Tub60D* (EGFRλ Tub60D-KD
379 condition) is sufficient to induce intrabasal growth (Fig. 6I-I', Fig. 6J, right columns), but
380 overall has no effect on formation of extra-epithelial tumors (Fig. 6J, left columns).
381 Furthermore, these extra-epithelial tumors remain unchanged compared to the other tested
382 conditions (Fig. S6). Thus, in this condition as well, intrabasal growth represents an inducible
383 program that is completely independent of extra-epithelial tumor formation.

384 Furthermore, in the EGFRλ Tub60D-KD condition, intrabasal tumors do not proliferate more
385 than epithelial clones (Fig. 6K). Lack of β3 Tubulin therefore appears as a major determinant
386 of intrabasal growth but does not promote any advantage by itself, even in a tumoral context.
387 This indicates that the ability to achieve escape relies, in the drosophila accessory gland, on
388 ecdysone signaling deprivation and not merely on the ability of tumor cells to reach the
389 intrabasal compartment.

390 Discussion

391 The National Cancer Institute defines cancer by their abnormal cells dividing without control
392 and invading nearby tissues. Epithelial cancers represent ~90% of all cancers (Bray et al.,
393 2018). As epithelial cells rest on a strong extracellular matrix on their basal side, epithelial
394 tumor cells must cross this basement membrane to invade nearby tissues. This is why this step
395 of invasion is called basal extrusion. Little is known about basal extrusion when it occurs
396 physiologically during development and when it occurs in the pathophysiological context of

397 tumorigenesis. Basal extrusion appears as a complex process: it can be induced by the clonal
398 expression of different oncogenes (Anton et al., 2018; Rambur et al., 2020; Villeneuve et al.,
399 2019); may occur in balance with apical extrusion (Anton et al., 2018; Marshall et al., 2011;
400 Ventrella et al., 2023); relies on multiple signaling pathways such as Notch (Ventrella et al.,
401 2023), Ras/MAPK and PI3K/Akt (Rambur et al., 2020) or PKC activation (Villeneuve et al.,
402 2019); depends on cholesterol uptake (Vialat et al., 2024) and lipid raft activity (Kajiwara et
403 al., 2022); and can be promoted by extracellular matrix degradation even though,
404 counterintuitively, this does not seem to be a necessary step (Shen et al., 2014). It also
405 depends on profound remodeling of cytoskeletal organization and of cell-cell and cell-matrix
406 interactions (Chountala et al., 2012; Ganier et al., 2018; Melo et al., 2023; Slattum et al.,
407 2009; Villeneuve et al., 2019). Overall, our data indicate that basal extrusion of tumor cells
408 appears furthermore as a two-fate phenomenon that, in drosophila accessory gland, is tightly
409 regulated by ecdysone signaling, as downregulation of this signaling induces growth of
410 intrabasal tumors. Interestingly, clonal expression of an oncogene in mouse epithelia induces
411 formation of dome-like structures where tumor cells accumulate at the same localization,
412 showing that this precise tumor fate also exists in mammals (Shirai et al., 2022). This
413 localization has long been known to favor tumor growth, as exemplified by the widespread
414 use of subcapsular renal xenografting in cancer research (Bogden et al., 1979). Moreover, in a
415 mouse model of intraductal human breast carcinogenesis, Zoeller et al demonstrated that
416 tumor cells adjacent to the basement membrane display extra-resistance to treatments when
417 compared with others, indicating that this specific microenvironment is most conducive to
418 survival upon treatment (Zoeller et al., 2017). An ability for tumor cells to reach this
419 compartment could then confer them a higher chance of survival and progression.
420 However, we were able to push tumor cell growth in this compartment by manipulating
421 *Tub60D* expression. In this case, no increase in cell proliferation and no apparent cell

422 disorganization are associated with intrabasal growth. Thus, by itself, growth in the intrabasal
423 compartment is not sufficient for tumor progression in the accessory gland.

424 Conversely, in this context, tumor cell resistance is actively induced by decreased canonical
425 ecdysone signaling. And, in human, we also show that AR signaling decreases with prostate
426 cancer progression. This lack of AR signaling also favors the most aggressive NEPC (Turpin
427 et al., 2023). In breast cancer, ER loss is a common event largely associated with tumor
428 aggressiveness (Kuukasjärvi et al., 1996). In prostate cancer, in the numerous alterations that
429 can affect AR, many mutations found in tumors are loss of function (Hay and McEwan,
430 2012). Moreover, in human, Androgen Deprivation Therapy (ADT) shows opposite effects
431 depending on cancer stage. For poorly differentiated or metastatic tumors, ADT has largely
432 proven its efficacy by increasing patient survival. However, for localized prostate cancer,
433 some studies argue that ADT displays no beneficial effect and is even associated with worse
434 outcome than active surveillance for patient survival (Lu-Yao et al., 2008; Merglen et al.,
435 2007). In men with hypogonadism, testosterone supplementation therapy has been feared to
436 increase prostate cancer risk. However, reviews of the scientific literature show no increase in
437 prostate cancer incidence with this treatment (Dupree et al., 2014; Michaud et al., 2015).
438 Finally, in High-Grade Prostate Intraepithelial Neoplasia (HGPIN), low testosterone
439 correlates with an increased risk of prostate cancer development (García-Cruz et al., 2012).
440 This suggests that decreased activity of sex steroid signaling in the early phases of
441 tumorigenesis could be implicated in cancer progression and/or the genesis of tumor cells
442 populations escaping endocrine therapy. In this context, to link changes in basal extrusion, sex
443 steroids and aggressiveness, it is noteworthy that particularly aggressive forms of ductal
444 carcinoma *in situ* in breast (Baqai and Shousha, 2003) and intraductal cancers in prostate
445 display both a growth initially restricted to the epithelial compartment and defects in sex
446 steroid signaling (Zhao et al., 2018). Thus, lack of sex steroid signaling could potentially

447 induce progression and escape to sex steroid deprivation in some endocrine-dependent forms
448 of cancer.
449 Overall, we show *in vivo* that epithelial basal extrusion is a complex phenomenon: cells can
450 extrude basally from the epithelium but still remain in the epithelial compartment. We show
451 that repression of sex steroid signaling in an oncogenic context induces a specific change in
452 tumor cell fate, in which these cells grow in a newly unveiled intrabasal compartment. We
453 show that, for tumor cells of the drosophila accessory gland, this represents a key event in the
454 genesis of tumors escaping sex steroid deprivation. Epithelial basal extrusion could therefore
455 be a key event in tumor escape and progression, depending on activity of specific pathways
456 such as sex steroid signaling.

457

458 ## Materials and Methods

459 **Fly stocks and experimental crosses**

460 y,w,HS:flp122/+;Act:FRTstopFRTGal4, UAS:GFP/CyO flies allowed conditional clonal
461 expression of GFP. Combination with UAS:EgfrλTop (#59843) allowed conditional clonal co-
462 expression of GFP and Egfrλtop (EGFRλ flies). EGFRλ flies were then crossed with following
463 stocks to realize experiments: UAS-GFP.nls (#4775, control condition), UAS-EcR RNAi
464 (#50712), UAS-Shd RNAi (#67456), UAS-Hr3 RNAi (#27253), UAS-Hr4 RNAi (#54803),
465 UAS-Sad RNAi (#67352), UAS-Phm RNAi (#65017), UAS-Tub60D RNAi (#64856) from the
466 Bloomington Stock Center.

467 **Conditional expression induction**

468 Briefly, flippase (flp)/FRT system was activated by a 12 min heat-shock induction at 37°C
469 during the pupal stage, to create an average of 4–6 clones per accessory gland (≈1% of total
470 number of epithelial cells). Flies were then kept at 27 °C until the end of pupal stage. Males

471 were collected at emergence from pupae 3 to 3.5 days after heat shock and kept for another 1
472 to 5 days at 27 °C before dissection.

473 **Immunohistochemistry and imaging**

474 Accessory glands were dissected in PBS, fixed for 10 min in 4% paraformaldehyde, washed
475 and permeabilized for 15 min in PBS containing 0.2% Triton (PBS-T). Glands were blocked
476 for one hour with 0.5% of BSA in PBS-T then incubated overnight at 4°C with primary
477 antibodies diluted in the same blocking solution. After three washes in PBS-T, glands were
478 incubated in secondary antibody diluted 1:1000 in blocking solution for 1 hour at room
479 temperature with DAPI (DiAminidoPhenylIndol, D8417, Sigma) 1:1000 (DNA staining)
480 and/or Alexa633-phalloidin (A22284, Life Technology) 1:5000 (to reveal F-actin). Glands
481 were then washed twice in PBS-T, once in PBS and subsequently mounted in Vectashield (#-
482 1000, Vector Laboratories). Imaging was realized on Leica SP8 confocal microscope, and
483 image stacks were processed either in ImageJ or Imaris software. All stainings were repeated a
484 minimum of 3 times on independent experiments.

485 List of antibodies: Mouse Coracle (1:300, #C566.9 DSHB), mouse Fasciclin III (1:400, #7G10
486 DSHB), goat GFP (1:1000, #5450 Abcam), rabbit pSrc (1:500, #44-660G Invitrogen), rabbit
487 pH3 (1:500, #06-570, Merck Millipore), rabbit cleaved-caspase 3 (1:400, #9661S, Cell
488 Signaling), secondary antibodies coupled to different fluorophores 488 (1:1000, A11055
489 Invitrogen), Cy3 or Cy5 (1:1000, 711-165-152, 715-165-151, 715-175-150, Jackson
490 Immunology).

491 **Clones sizes, cells and nuclei size and numbers, proliferation rate**

492 Clones/tumors sizes, cells and nuclei volumes and numbers were determined from 3D
493 reconstruction and automatic quantification in Imaris software. For each clone/tumor, average
494 cell size was determined by ratio between clone size and number of nuclei in the considered

495 clone. Proliferation rate was calculated compared to number of cells in a clone expressing GFP
496 only (as in Fig. S3A). A typical clone is composed of 2 cells, and so 2 cells was taken as 100%
497 proliferation. See Table 2 for the number of experiments and total numbers of individual flies
498 that were processed for each experiment.

499 **Extra-epithelial or intrabasal tumor frequency**

500 Extra-epithelial tumor frequency was determined as the percentage of flies that displayed at
501 least one tumor on their accessory glands at dissection. For intrabasal tumors, individual glands
502 were considered. See Table 2 for the number of experiments and total numbers of individual
503 flies that were processed for each experiment.

504 **RNA FISH**

505 Single-molecule RNA fluorescence in situ hybridization (smRNA-FISH) for transcripts of EcR
506 from the accessory gland was performed using Stellaris probes (Biosearch Technologies).
507 Probe sequences are listed in table S1. Accessory gland were dissected in PBS and fixed in 4%
508 formaldehyde, 0.3% Triton X-100, 1x PBS for 20 min at room temperature, rinsed and
509 permeabilized in 70% ethanol at 4°C overnight. Glands were rehydrated in smRNA FISH wash
510 buffer (10% formamide in 2x SSC) for 10 min, resuspended in 50µL hybridization buffer (10%
511 dextran sulphate, 10% formamide in 2xSSC) supplemented with 1.5µL of smRNA FISH
512 probes. Hybridization was performed at 37°C overnight. Glands were then washed twice with
513 smRNA FISH wash buffer at 37°C for 30 min and twice with 2xSSC solution. Then, DNA was
514 stained with DAPI (1/500 dilution in 2x SSC) at room temperature for 20 min. Accessory glands
515 were then mounted in 30µL Vectashield prior to imaging. The resulting images were processed
516 using FIJI/ImageJ.

517 **Statistical analyses and human data**

518 All experiments were repeated independently a minimum of three times (N: number of
519 independent experiments) on numerous glands (n: number of pairs of glands or number of
520 imaged and quantified glands for tumor size and nuclei number quantification; see Table 2).
521 Statistical analyses were performed using GraphPad Prism 6 for tumor size and nuclei number
522 quantification were compared by Krustal-Wallis test; % of glands with extra-glandular tumors
523 were compared by Chi2 test; gene expression in qPCR was compared by two-tailed impaired
524 T-test. Human data processing was done using the tools developed by Theurillat et al. and
525 available at prostatecanceratlas.org. Expression data and pseudotime progression were
526 individually retrieved for each considered gene using the Explore/bulk RNA function, and were
527 grouped by stage (NORMAL, 173 samples, PRIMARY, 708 samples, mCRPC, 484 samples).
528 Statistical analyses were then performed using GraphPad Prism 6 and quantifications were
529 compared by Mann-Whitney test.

530 In all figures, significance is described as follows : * $p<0.05$; ** $p<0.01$; *** $p<0.001$; ****
531 $p<0.0001$.

532 **Acknowledgments:** The authors thank N. Anglaret, L. Babkina, A. De Haze, C. Gaudichet
533 and C. Tamisier for technical help; Dr E. Chautard and Dr A. Bruhat for scientific advices;
534 Bloomington Drosophila Stock Center (BDSC) for providing fly stocks, and Drosophila
535 Studies Hybridoma Bank (DSHB) for providing antibodies. Dr Krzysztof Jagla for kind gift
536 of β3 tubulin antibody. CLermont Imagerie Confocale (CLIC) facility for support with
537 imaging. J-P Theurillat, S. Nicastri and the Prostate Cancer Atlas team for adding a new tool
538 upon request.

539 **Funding:** this study was funded by La ligue contre le cancer (CJ), La Fondation ARC (MV),
540 French Center for the 3Rs (FC3R) grant Re-Innov (CJ).

541 **Conflict of interest:** Authors declare that they have no competing interests.

References

Abida W, Cyrta J, Heller G, Prandi D, Armenia J, Coleman I, Cieslik M, Benelli M, Robinson D, Van Allen EM, Sboner A, Fedrizzi T, Mosquera JM, Robinson BD, De Sarkar N, Kunju LP, Tomlins S, Wu YM, Nava Rodrigues D, Loda M, Gopalan A, Reuter VE, Pritchard CC, Mateo J, Bianchini D, Miranda S, Carreira S, Rescigno P, Filipenko J, Vinson J, Montgomery RB, Beltran H, Heath EI, Scher HI, Kantoff PW, Taplin M-E, Schultz N, DeBono JS, Demichelis F, Nelson PS, Rubin MA, Chinnaiyan AM, Sawyers CL. 2019. Genomic correlates of clinical outcome in advanced prostate cancer. Proceedings of the National Academy of Sciences of the United States of America **116**:11428–11436. DOI: https://doi.org/10.1073/pnas.1902651116, PMID: 31061129

Andersson S, Berman DM, Jenkins EP, Russell DW. 1991. Deletion of steroid 5 alpha-reductase 2 gene in male pseudohermaphroditism. Nature **354**:159–161. DOI: https://doi.org/10.1038/354159a0, PMID: 1944596

Anton KA, Kajita M, Narumi R, Fujita Y, Tada M. 2018. Src-transformed cells hijack mitosis to extrude from the epithelium. Nature communications **9**:4695. DOI: https://doi.org/10.1038/s41467-018-07163-4, PMID: 30410020

Arora VK, Schenkein E, Murali R, Subudhi SK, Wongvipat J, Balbas MD, Shah N, Cai L, Efstathiou E, Logothetis C, Zheng D, Sawyers CL. 2013. Glucocorticoid receptor confers resistance to antiandrogens by bypassing androgen receptor blockade. Cell **155**:1309–1322. DOI: https://doi.org/10.1016/j.cell.2013.11.012, PMID: 24315100

Atashzar MR, Baharlou R, Karami J, Abdollahi H, Rezaei R, Pourramezan F, Zoljalali Moghaddam SH. 2020. Cancer stem cells: A review from origin to therapeutic implications. Journal of cellular physiology **235**:790–803. DOI: https://doi.org/10.1002/jcp.29044, PMID: 31286518

Bangi E, Ang C, Smibert P, Uzilov AV, Teague AG, Antipin Y, Chen R, Hecht C, Gruszczynski N, Yon WJ, Malyshev D, Laspina D, Selkridge I, Rainey H, Moe AS, Lau CY, Taik P, Wilck E, Bhardwaj A, Sung M, Kim S, Yum K, Sebra R, Donovan M, Misiukiewicz K, Schadt EE, Posner MR, Cagan RL. 2019. A personalized platform identifies trametinib plus zoledronate for a patient with KRAS-mutant metastatic colorectal cancer. Science advances **5**:eaav6528. DOI: https://doi.org/10.1126/sciadv.aav6528, PMID: 31131321

Bangi E, Murgia C, Teague AGS, Sansom OJ, Cagan RL. 2016. Functional exploration of colorectal cancer genomes using Drosophila. Nature communications **7**:13615. DOI: https://doi.org/10.1038/ncomms13615, PMID: 27897178

Baqai T, Shousha S. 2003. Oestrogen receptor negativity as a marker for high-grade ductal carcinoma in situ of the breast. Histopathology **42**:440–447. DOI: https://doi.org/10.1046/j.1365-2559.2003.01612.x, PMID: 12713620

Barbieri CE, Baca SC, Lawrence MS, Demichelis F, Blattner M, Theurillat J-P, White TA, Stojanov P, Van Allen E, Stransky N, Nickerson E, Chae S-S, Boysen G, Auclair D, Onofrio RC, Park K, Kitabayashi N, MacDonald TY, Sheikh K, Vuong T, Guiducci C, Cibulskis K, Sivachenko A, Carter SL, Saksena G, Voet D, Hussain WM, Ramos AH, Winckler W, Redman MC, Ardlie K, Tewari AK, Mosquera JM, Rupp N, Wild PJ, Moch H, Morrissey C, Nelson PS, Kantoff PW, Gabriel SB, Golub TR, Meyerson M, Lander ES, Getz G, Rubin MA, Garraway LA. 2012. Exome sequencing identifies recurrent SPOP, FOXA1 and MED12 mutations in prostate cancer. Nature genetics **44**:685–689. DOI: https://doi.org/10.1038/ng.2279, PMID: 22610119

Baumgartner M, Radziwill G, Lorger M, Weiss A, Moelling K. 2008. c-Src-mediated epithelial cell migration and invasion regulated by PDZ binding site. Molecular and cellular biology **28**:642–55. DOI: https://doi.org/10.1128/MCB.01024-07, PMID: 18039857

Beltran H, Prandi D, Mosquera JM, Benelli M, Puca L, Cyrta J, Marotz C, Giannopoulou E, Chakravarthi BVSK, Varambally S, Tomlins SA, Nanus DM, Tagawa ST, Van Allen EM, Elemento O, Sboner A, Garraway LA, Rubin MA, Demichelis F. 2016. Divergent clonal evolution of castration-resistant neuroendocrine prostate cancer. Nature medicine **22**:298–305. DOI: https://doi.org/10.1038/nm.4045, PMID: 26855148

Bhatia-Gaur R, Donjacour AA, Sciavolino PJ, Kim M, Desai N, Young P, Norton CR, Gridley T, Cardiff RD, Cunha GR, Abate-Shen C, Shen MM. 1999. Roles for Nkx3.1 in prostate development and cancer. Genes & development **13**:966–977. DOI: https://doi.org/10.1101/gad.13.8.966, PMID: 10215624

Bogden AE, Haskell PM, LePage DJ, Kelton DE, Cobb WR, Esber HJ. 1979. Growth of human tumor xenografts implanted under the renal capsule of normal immunocompetent mice. Experimental cell biology **47**:281–293. DOI: https://doi.org/10.1159/000162947, PMID: 467773

Bolis M, Bossi D, Vallerga A, Ceserani V, Cavalli M, Impellizzieri D, Di Rito L, Zoni E, Mosole S, Elia AR, Rinaldi A, Pereira Mestre R, D'Antonio E, Ferrari M, Stoffel F, Jermini F, Gillessen S, Bubendorf L, Schraml P, Calcinotto A, Corey E, Moch H, Spahn M, Thalmann G, Kruithof-de Julio M, Rubin MA, Theurillat J-PP. 2021. Dynamic prostate cancer transcriptome analysis delineates the trajectory to

601 disease progression. Nature communications **12**:7033. DOI: https://doi.org/10.1038/s41467-021-26840-
602 5, PMID: 34857732
603 Boysen G, Barbieri CE, Prandi D, Blattner M, Chae S-S, Dahija A, Nataraj S, Huang D, Marotz C, Xu L, Huang
604 J, Lecca P, Chhangawala S, Liu D, Zhou P, Sboner A, de Bono JS, Demichelis F, Houvras Y, Rubin
605 MA. 2015. SPOP mutation leads to genomic instability in prostate cancer. eLife **4**. DOI:
606 https://doi.org/10.7554/eLife.09207, PMID: 26374986
607 Bray F, Ferlay J, Soerjomataram I, Siegel RL, Torre LA, Jemal A. 2018. Global cancer statistics 2018:
608 GLOBOCAN estimates of incidence and mortality worldwide for 36 cancers in 185 countries. CA: a
609 cancer journal for clinicians **68**:394–424. DOI: https://doi.org/10.3322/caac.21492, PMID: 30207593
610 Bruhat A, Tourmente S, Chapel S, Sobrier ML, Couderc JL, Dastugue B. 1990. Regulatory elements in the first
611 intron contribute to transcriptional regulation of the beta 3 tubulin gene by 20-hydroxyecdysone in
612 Drosophila Kc cells. Nucleic acids research **18**:2861–2867. DOI:
613 https://doi.org/10.1093/nar/18.10.2861, PMID: 2349088
614 Cai C, Chen Sen, Ng P, Bubley GJ, Nelson PS, Mostaghel EA, Marck B, Matsumoto AM, Simon NI, Wang H,
615 Chen Shaoyong, Balk SP. 2011. Intratumoral de novo steroid synthesis activates androgen receptor in
616 castration-resistant prostate cancer and is upregulated by treatment with CYP17A1 inhibitors. Cancer
617 research **71**:6503–6513. DOI: https://doi.org/10.1158/0008-5472.CAN-11-0532, PMID: 21868758
618 Cancer Genome Atlas Research Network TCGAR, Cancer Genome Atlas Research Network A, Ahn J, Akbani
619 R, Ally A, Amin S, Andry CD, Annala M, Aprikian A, Armenia J, Arora A, Auman JT, Balasundaram
620 M, Balu S, Barbieri CE, Bauer T, Benz CC, Bergeron A, Beroukhim R, Berrios M, Bivol A,
621 Bodenheimer T, Boice L, Bootwalla MS, Borges dos Reis R, Boutros PC, Bowen J, Bowlby R, Boyd J,
622 Bradley RK, Breggia A, Brimo F, Bristow CA, Brooks D, Broom BM, Bryce AH, Bubley G, Burks E,
623 Butterfield YSN, Button M, Canes D, Carlotti CG, Carlsen R, Carmel M, Carroll PR, Carter SL, Cartun
624 R, Carver BS, Chan JM, Chang MT, Chen Y, Cherniack AD, Chevalier S, Chin L, Cho J, Chu A,
625 Chuah E, Chudamani S, Cibulskis K, Ciriello G, Clarke A, Cooperberg MR, Corcoran NM, Costello
626 AJ, Cowan J, Crain D, Curley E, David K, Demchok JA, Demichelis F, Dhalla N, Dhir R, Doueik A,
627 Drake B, Dvinge H, Dyakova N, Felau I, Ferguson ML, Frazer S, Freedland S, Fu Y, Gabriel SB, Gao
628 J, Gardner J, Gastier-Foster JM, Gehlenborg N, Gerken M, Gerstein MB, Getz G, Godwin AK, Gopalan
629 A, Graefen M, Graim K, Gribbin T, Guin R, Gupta M, Hadjipanayis A, Haider S, Hamel L, Hayes DN,
630 Heiman DI, Hess J, Hoadley KA, Holbrook AH, Holt RA, Holway A, Hovens CM, Hoyle AP, Huang
631 M, Hutter CM, Ittmann M, Iype L, Jefferys SR, Jones CD, Jones SJM, Juhl H, Kahles A, Kane CJ,
632 Kasaian K, Kerger M, Khurana E, Kim J, Klein RJ, Kucherlapati R, Lacombe L, Ladanyi M, Lai PH,
633 Laird PW, Lander ES, Latour M, Lawrence MS, Lau K, LeBien T, Lee D, Lee S, Lehmann K-V, Leraas
634 KM, Leshchiner I, Leung R, Libertino JA, Lichtenberg TM, Lin P, Linehan WM, Ling S, Lippman SM,
635 Liu J, Liu W, Lochovsky L, Loda M, Logothetis C, Lolla L, Longacre T, Lu Y, Luo J, Ma Y,
636 Mahadeshwar HS, Mallery D, Mariamidze A, Marra MA, Mayo M, McCall S, McKercher G, Meng S,
637 Mes-Masson A-M, Merino MJ, Meyerson M, Mieczkowski PA, Mills GB, Shaw KRM, Minner S,
638 Moinzadeh A, Moore RA, Morris S, Morrison C, Mose LE, Mungall AJ, Murray BA, Myers JB, Naresh
639 R, Nelson J, Nelson MA, Nelson PS, Newton Y, Noble MS, Noushmehr H, Nykter M, Pantazi A,
640 Parfenov M, Park PJ, Parker JS, Paulauskis J, Penny R, Perou CM, Piché A, Pihl T, Pinto PA, Prandi D,
641 Protopopov A, Ramirez NC, Rao A, Rathmell WK, Rätsch G, Ren X, Reuter VE, Reynolds SM, Rhie
642 SK, Rieger-Christ K, Roach J, Robertson AG, Robinson B, Rubin MA, Saad F, Sadeghi S, Saksena G,
643 Saller C, Salner A, Sanchez-Vega F, Sander C, Sandusky G, Sauter G, Sboner A, Scardino PT, Scarlata
644 E, Schein JE, Schlomm T, Schmidt LS, Schultz N, Schumacher SE, Seidman J, Neder L, Seth S, Sharp
645 A, Shelton C, Shelton T, Shen H, Shen R, Sherman M, Sheth M, Shi Y, Shih J, Shmulevich I, Simko J,
646 Simon R, Simons JV, Sipahimalani P, Skelly T, Sofia HJ, Soloway MG, Song X, Sorcini A, Sougnez C,
647 Stepa S, Stewart C, Stewart J, Stuart JM, Sullivan TB, Sun C, Sun H, Tam A, Tan D, Tang J, Tarnuzzer
648 R, Tarvin K, Taylor BS, Teebagy P, Tenggara I, Têtu B, Tewari A, Thiessen N, Thompson T, Thorne
649 LB, Tirapelli DP, Tomlins SA, Trevisan FA, Troncoso P, True LD, Tsourlakis MC, Tyekucheva S, Van
650 Allen E, Van Den Berg DJ, Veluvolu U, Verhaak R, Vocke CD, Voet D, Wan Y, Wang Q, Wang W,
651 Wang Z, Weinhold N, Weinstein JN, Weisenberger DJ, Wilkerson MD, Wise L, Witte J, Wu C-C, Wu
652 J, Wu Y, Xu AW, Yadav SS, Yang LL, Yang LL, Yau C, Ye H, Yena P, Zeng T, Zenklusen JC, Zhang
653 H, Zhang JJ, Zhang JJ, Zhang W, Zhong Y, Zhu K, Zmuda E, Abeshouse A, Ahn J, Akbani R, Ally A,
654 Amin S, Andry CD, Annala M, Aprikian A, Armenia J, Arora A, Auman JT, Balasundaram M, Balu S,
655 Barbieri CE, Bauer T, Benz CC, Bergeron A, Beroukhim R, Berrios M, Bivol A, Bodenheimer T, Boice
656 L, Bootwalla MS, Borges dos Reis R, Boutros PC, Bowen J, Bowlby R, Boyd J, Bradley RK, Breggia
657 A, Brimo F, Bristow CA, Brooks D, Broom BM, Bryce AH, Bubley G, Burks E, Butterfield YSN,
658 Button M, Canes D, Carlotti CG, Carlsen R, Carmel M, Carroll PR, Carter SL, Cartun R, Carver BS,
659 Chan JM, Chang MT, Chen Y, Cherniack AD, Chevalier S, Chin L, Cho J, Chu A, Chuah E,
660 Chudamani S, Cibulskis K, Ciriello G, Clarke A, Cooperberg MR, Corcoran NM, Costello AJ, Cowan

661 J, Crain D, Curley E, David K, Demchok JA, Demichelis F, Dhalla N, Dhir R, Doueik A, Drake B,
662 Dvinge H, Dyakova N, Felau I, Ferguson ML, Frazer S, Freedland S, Fu Y, Gabriel SB, Gao J, Gardner
663 J, Gastier-Foster JM, Gehlenborg N, Gerken M, Gerstein MB, Getz G, Godwin AK, Gopalan A,
664 Graefen M, Graim K, Gribbin T, Guin R, Gupta M, Hadjipanayis A, Haider S, Hamel L, Hayes DN,
665 Heiman DI, Hess J, Hoadley KA, Holbrook AH, Holt RA, Holway A, Hovens CM, Hoyle AP, Huang
666 M, Hutter CM, Ittmann M, Iype L, Jefferys SR, Jones CD, Jones SJM, Juhl H, Kahles A, Kane CJ,
667 Kasaian K, Kerger M, Khurana E, Kim J, Klein RJ, Kucherlapati R, Lacombe L, Ladanyi M, Lai PH,
668 Laird PW, Lander ES, Latour M, Lawrence MS, Lau K, LeBien T, Lee D, Lee S, Lehmann K-V, Leraas
669 KM, Leshchiner I, Leung R, Libertino JA, Lichtenberg TM, Lin P, Linehan WM, Ling S, Lippman SM,
670 Liu J, Liu W, Lochovsky L, Loda M, Logothetis C, Lolla L, Longacre T, Lu Y, Luo J, Ma Y,
671 Mahadeshwar HS, Mallery D, Mariamidze A, Marra MA, Mayo M, McCall S, McKercher G, Meng S,
672 Mes-Masson A-M, Merino MJ, Meyerson M, Mieczkowski PA, Mills GB, Shaw KRM, Minner S,
673 Moinzadeh A, Moore RA, Morris S, Morrison C, Mose LE, Mungall AJ, Murray BA, Myers JB, Naresh
674 R, Nelson J, Nelson MA, Nelson PS, Newton Y, Noble MS, Noushmehr H, Nykter M, Pantazi A,
675 Parfenov M, Park PJ, Parker JS, Paulauskis J, Penny R, Perou CM, Piché A, Pihl T, Pinto PA, Prandi D,
676 Protopopov A, Ramirez NC, Rao A, Rathmell WK, Rätsch G, Ren X, Reuter VE, Reynolds SM, Rhie
677 SK, Rieger-Christ K, Roach J, Robertson AG, Robinson B, Rubin MA, Saad F, Sadeghi S, Saksena G,
678 Saller C, Salner A, Sanchez-Vega F, Sander C, Sandusky G, Sauter G, Sboner A, Scardino PT, Scarlata
679 E, Schein JE, Schlomm T, Schmidt LS, Schultz N, Schumacher SE, Seidman J, Neder L, Seth S, Sharp
680 A, Shelton C, Shelton T, Shen H, Shen R, Sherman M, Sheth M, Shi Y, Shih J, Shmulevich I, Simko J,
681 Simon R, Simons JV, Sipahimalani P, Skelly T, Sofia HJ, Soloway MG, Song X, Sorcini A, Sougnez C,
682 Stepa S, Stewart C, Stewart J, Stuart JM, Sullivan TB, Sun C, Sun H, Tam A, Tan D, Tang J, Tarnuzzer
683 R, Tarvin K, Taylor BS, Teebagy P, Tenggara I, Têtu B, Tewari A, Thiessen N, Thompson T, Thorne
684 LB, Tirapelli DP, Tomlins SA, Trevisan FA, Troncoso P, True LD, Tsourlakis MC, Tyekucheva S, Van
685 Allen E, Van Den Berg DJ, Veluvolu U, Verhaak R, Vocke CD, Voet D, Wan Y, Wang Q, Wang W,
686 Wang Z, Weinhold N, Weinstein JN, Weisenberger DJ, Wilkerson MD, Wise L, Witte J, Wu C-C, Wu
687 J, Wu Y, Xu AW, Yadav SS, Yang LL, Yang LL, Yau C, Ye H, Yena P, Zeng T, Zenklusen JC, Zhang
688 H, Zhang JJ, Zhang JJ, Zhang W, Zhong Y, Zhu K, Zmuda E. 2015. No Title. Cell **163**. DOI:
689 https://doi.org/10.1016/j.cell.2015.10.025, PMID: 26544944
690 Cao B, Qi Y, Zhang G, Xu D, Zhan Y, Alvarez X, Guo Z, Fu X, Plymate SR, Sartor O, Zhang H, Dong Y. 2014.
691 Androgen receptor splice variants activating the full-length receptor in mediating resistance to
692 androgen-directed therapy. Oncotarget **5**:1646–1656. DOI: https://doi.org/10.18632/oncotarget.1802,
693 PMID: 24722067
694 Carney GE, Wade AA, Sapra R, Goldstein ES, Bender M. 1997. DHR3, an ecdysone-inducible early-late gene
695 encoding a Drosophila nuclear receptor, is required for embryogenesis. Proceedings of the National
696 Academy of Sciences of the United States of America **94**:12024–12029. DOI:
697 https://doi.org/10.1073/pnas.94.22.12024, PMID: 9342356
698 Chountala M, Vakaloglou KM, Zervas CG. 2012. Parvin overexpression uncovers tissue-specific genetic
699 pathways and disrupts F-actin to induce apoptosis in the developing epithelia in Drosophila. PloS one
700 **7**:e47355. DOI: https://doi.org/10.1371/journal.pone.0047355, PMID: 23077599
701 Clarke R, Brünner N, Katzenellenbogen BS, Thompson EW, Norman MJ, Koppi C, Paik S, Lippman ME,
702 Dickson RB. 1989. Progression of human breast cancer cells from hormone-dependent to hormone-
703 independent growth both in vitro and in vivo. Proceedings of the National Academy of Sciences of the
704 United States of America **86**:3649–3653. DOI: https://doi.org/10.1073/pnas.86.10.3649, PMID:
705 2726742
706 Dowsett M, Smith IE, Ebbs SR, Dixon JM, Skene A, Griffith C, Boeddinghaus I, Salter J, Detre S, Hills M,
707 Ashley S, Francis S, Walsh G, A'Hern R. 2006. Proliferation and apoptosis as markers of benefit in
708 neoadjuvant endocrine therapy of breast cancer. Clinical cancer research : an official journal of the
709 American Association for Cancer Research **12**:1024s–1030s. DOI: https://doi.org/10.1158/1078-
710 0432.CCR-05-2127, PMID: 16467120
711 Dupree JM, Langille GM, Khera M, Lipshultz LI. 2014. The safety of testosterone supplementation therapy in
712 prostate cancer. Nature reviews. Urology **11**:526–530. DOI: https://doi.org/10.1038/nrurol.2014.163,
713 PMID: 25069737
714 Ganier O, Schnerch D, Nigg EA. 2018. Structural centrosome aberrations sensitize polarized epithelia to basal
715 cell extrusion. Open Biology **8**:180044. DOI: https://doi.org/10.1098/rsob.180044, PMID: 29899122
716 García-Cruz E, Piqueras M, Ribal MJ, Huguet J, Serapiao R, Peri L, Izquierdo L, Alcaraz A. 2012. Low
717 testosterone level predicts prostate cancer in re-biopsy in patients with high grade prostatic
718 intraepithelial neoplasia. BJU international **110**:E199-202. DOI: https://doi.org/10.1111/j.1464-
719 410X.2011.10876.x, PMID: 22257176

720 Gauhar Z, Sun LV, Hua S, Mason CE, Fuchs F, Li T-R, Boutros M, White KP. 2009. Genomic mapping of
721 binding regions for the Ecdysone receptor protein complex. Genome research **19**:1006–1013. DOI:
722 https://doi.org/10.1101/gr.081349.108, PMID: 19237466
723 Geller J, Albert J, Loza D, Geller S, Stoeltzing W, de la Vega D. 1978. DHT concentrations in human prostate
724 cancer tissue. The Journal of Clinical Endocrinology and Metabolism **46**:440–444. DOI:
725 https://doi.org/10.1210/jcem-46-3-440, PMID: 87401
726 Hanahan D, Weinberg RA. 2011. Hallmarks of cancer: the next generation. Cell **144**:646–674. DOI:
727 https://doi.org/10.1016/j.cell.2011.02.013, PMID: 21376230
728 Hay CW, McEwan IJ. 2012. The impact of point mutations in the human androgen receptor: classification of
729 mutations on the basis of transcriptional activity. PloS one **7**:e32514. DOI:
730 https://doi.org/10.1371/journal.pone.0032514, PMID: 22403669
731 Humphrey PA. 2012. Histological variants of prostatic carcinoma and their significance. Histopathology **60**:59–
732 74. DOI: https://doi.org/10.1111/j.1365-2559.2011.04039.x
733 Isaacs JT, Furuya Y, Berges R. 1994. The role of androgen in the regulation of programmed cell death/apoptosis
734 in normal and malignant prostatic tissue. Seminars in cancer biology **5**:391–400. PMID: 7849267
735 Ito S, Ueda T, Ueno A, Nakagawa H, Taniguchi H, Kayukawa N, Miki T. 2014. A genetic screen in Drosophila
736 for regulators of human prostate cancer progression. Biochemical and Biophysical Research
737 Communications **451**:548–555. DOI: https://doi.org/10.1016/j.bbrc.2014.08.015, PMID: 25117438
738 Iwasa Y, Mizokami A, Miwa S, Koshida K, Namiki M. 2007. Establishment and characterization of androgen-
739 independent human prostate cancer cell lines, LN-REC4 and LNCaP-SF, from LNCaP. International
740 journal of urology : official journal of the Japanese Urological Association **14**:233–239. DOI:
741 https://doi.org/10.1111/j.1442-2042.2007.01532.x, PMID: 17430262
742 Kajiwara K, Chen P-K, Abe Y, Okuda S, Kon S, Adachi J, Tomonaga T, Fujita Y, Okada M. 2022. Src
743 activation in lipid rafts confers epithelial cells with invasive potential to escape from apical extrusion
744 during cell competition. Current biology : CB **32**:3460-3476.e6. DOI:
745 https://doi.org/10.1016/j.cub.2022.06.038, PMID: 35809567
746 Kumar A, Coleman I, Morrissey C, Zhang X, True LD, Gulati R, Etzioni R, Bolouri H, Montgomery B, White
747 T, Lucas JM, Brown LG, Dumpit RF, DeSarkar N, Higano C, Yu EY, Coleman R, Schultz N, Fang M,
748 Lange PH, Shendure J, Vessella RL, Nelson PS. 2016. Substantial interindividual and limited
749 intraindividual genomic diversity among tumors from men with metastatic prostate cancer. Nature
750 medicine **22**:369–378. DOI: https://doi.org/10.1038/nm.4053, PMID: 26928463
751 Kuukasjärvi T, Kononen J, Helin H, Holli K, Isola J. 1996. Loss of estrogen receptor in recurrent breast cancer is
752 associated with poor response to endocrine therapy. Journal of clinical oncology : official journal of the
753 American Society of Clinical Oncology **14**:2584–2589. DOI:
754 https://doi.org/10.1200/JCO.1996.14.9.2584, PMID: 8823339
755 Labrecque MP, Coleman IM, Brown LG, True LD, Kollath L, Lakely B, Nguyen HM, Yang YC, da Costa
756 RMG, Kaipainen A, Coleman R, Higano CS, Yu EY, Cheng HH, Mostaghel EA, Montgomery B,
757 Schweizer MT, Hsieh AC, Lin DW, Corey E, Nelson PS, Morrissey C. 2019. Molecular profiling
758 stratifies diverse phenotypes of treatment-refractory metastatic castration-resistant prostate cancer. The
759 Journal of clinical investigation **129**:4492–4505. DOI: https://doi.org/10.1172/JCI128212, PMID:
760 31361600
761 Lapuk AV, Wu C, Wyatt AW, McPherson A, McConeghy BJ, Brahmbhatt S, Mo F, Zoubeidi A, Anderson S,
762 Bell RH, Haegert A, Shukin R, Wang Y, Fazli L, Hurtado-Coll A, Jones EC, Hach F, Hormozdiari F,
763 Hajirasouliha I, Boutros PC, Bristow RG, Zhao Y, Marra MA, Fanjul A, Maher CA, Chinnaiyan AM,
764 Rubin MA, Beltran H, Sahinalp SC, Gleave ME, Volik SV, Collins CC. 2012. From sequence to
765 molecular pathology, and a mechanism driving the neuroendocrine phenotype in prostate cancer. The
766 Journal of pathology **227**:286–297. DOI: https://doi.org/10.1002/path.4047, PMID: 22553170
767 Leiblich A, Marsden L, Gandy C, Corrigan L, Jenkins R, Hamdy F, Wilson C. 2012. Bone morphogenetic
768 protein- and mating-dependent secretory cell growth and migration in the Drosophila accessory gland.
769 Proceedings of the National Academy of Sciences **109**:19292–19297. DOI:
770 https://doi.org/10.1073/pnas.1214517109, PMID: 23129615
771 Levine BD, Cagan RL. 2016. Drosophila Lung Cancer Models Identify Trametinib plus Statin as Candidate
772 Therapeutic. Cell reports **14**:1477–1487. DOI: https://doi.org/10.1016/j.celrep.2015.12.105, PMID:
773 26832408
774 Locke JA, Guns ES, Lubik AA, Adomat HH, Hendy SC, Wood CA, Ettinger SL, Gleave ME, Nelson CC. 2008.
775 Androgen levels increase by intratumoral de novo steroidogenesis during progression of castration-
776 resistant prostate cancer. Cancer research **68**:6407–6415. DOI: https://doi.org/10.1158/0008-
777 5472.CAN-07-5997, PMID: 18676866

Lu-Yao GL, Albertsen PC, Moore DF, Shih W, Lin Y, DiPaola RS, Yao S-L. 2008. Survival following primary androgen deprivation therapy among men with localized prostate cancer. JAMA **300**:173–181. DOI: https://doi.org/10.1001/jama.300.2.173, PMID: 18612114

Marshall TW, Lloyd IE, Delalande JM, Näthke I, Rosenblatt J. 2011. The tumor suppressor adenomatous polyposis coli controls the direction in which a cell extrudes from an epithelium. Molecular Biology of the Cell **22**:3962–3970. DOI: https://doi.org/10.1091/mbc.E11-05-0469, PMID: 21900494

Melo S, Guerrero P, Moreira Soares M, Bordin JR, Carneiro F, Carneiro P, Dias MB, Carvalho J, Figueiredo J, Seruca R, Travasso RDM. 2023. The ECM and tissue architecture are major determinants of early invasion mediated by E-cadherin dysfunction. Communications Biology **6**:1132. DOI: https://doi.org/10.1038/s42003-023-05482-x, PMID: 37938268

Merglen A, Schmidlin F, Fioretta G, Verkooijen HM, Rapiti E, Zanetti R, Miralbell R, Bouchardy C. 2007. Short- and long-term mortality with localized prostate cancer. Archives of internal medicine **167**:1944–1950. DOI: https://doi.org/10.1001/archinte.167.18.1944, PMID: 17923593

Michaud JE, Billups KL, Partin AW. 2015. Testosterone and prostate cancer: an evidence-based review of pathogenesis and oncologic risk. Therapeutic advances in urology **7**:378–387. DOI: https://doi.org/10.1177/1756287215597633, PMID: 26622322

Miyoshi Y, Uemura H, Umemoto S, Sakamaki K, Morita S, Suzuki K, Shibata Y, Masumori N, Ichikawa T, Mizokami A, Sugimura Y, Nonomura N, Sakai H, Honma S, Harada M, Kubota Y. 2014. High testosterone levels in prostate tissue obtained by needle biopsy correlate with poor-prognosis factors in prostate cancer patients. BMC cancer **14**:717. DOI: https://doi.org/10.1186/1471-2407-14-717, PMID: 25256077

Molano-Fernández M, Hickson ID, Herranz H. 2022. Cyclin E overexpression in the Drosophila accessory gland induces tissue dysplasia. Frontiers in cell and developmental biology **10**:992253. DOI: https://doi.org/10.3389/fcell.2022.992253, PMID: 36704199

Nagabhushan M, Miller CM, Pretlow TP, Giaconia JM, Edgehouse NL, Schwartz S, Kung HJ, de Vere White RW, Gumerlock PH, Resnick MI, Amini SB, Pretlow TG. 1996. CWR22: the first human prostate cancer xenograft with strongly androgen-dependent and relapsed strains both in vivo and in soft agar. Cancer research **56**:3042–3046. PMID: 8674060

Petryk A, Warren JT, Marqués G, Jarcho MP, Gilbert LI, Kahler J, Parvy J-P, Li Y, Dauphin-Villemant C, O'Connor MB. 2003. Shade is the Drosophila P450 enzyme that mediates the hydroxylation of ecdysone to the steroid insect molting hormone 20-hydroxyecdysone. Proceedings of the National Academy of Sciences of the United States of America **100**:13773–13778. DOI: https://doi.org/10.1073/pnas.2336088100, PMID: 14610274

Rambur A, Lours-Calet C, Beaudoin C, Buñay J, Vialat M, Mirouse V, Trousson A, Renaud Y, Lobaccaro J-MA, Baron S, Morel L, de Joussineau C. 2020. Sequential Ras/MAPK and PI3K/AKT/mTOR pathways recruitment drives basal extrusion in the prostate-like gland of Drosophila. Nature communications **11**:2300. DOI: https://doi.org/10.1038/s41467-020-16123-w, PMID: 32385236

Rambur A, Vialat M, Beaudoin C, Lours-Calet C, Lobaccaro J-M, Baron S, Morel L, de Joussineau C. 2021. Drosophila Accessory Gland: A Complementary In Vivo Model to Bring New Insight to Prostate Cancer. Cells **10**. DOI: https://doi.org/10.3390/cells10092387, PMID: 34572036

Read RD. 2011. Drosophila melanogaster as a model system for human brain cancers. Glia **59**:1364–76. DOI: https://doi.org/10.1002/glia.21148, PMID: 21538561

Read RD, Cavenee WK, Furnari FB, Thomas JB. 2009. A Drosophila Model for EGFR-Ras and PI3K-Dependent Human Glioma. PLoS Genetics **5**:e1000374. DOI: https://doi.org/10.1371/journal.pgen.1000374

Rodriguez D, Ramkairsingh M, Lin X, Kapoor A, Major P, Tang D. 2019. The Central Contributions of Breast Cancer Stem Cells in Developing Resistance to Endocrine Therapy in Estrogen Receptor (ER)-Positive Breast Cancer. Cancers **11**. DOI: https://doi.org/10.3390/cancers11071028, PMID: 31336602

Rybak AP, Bristow RG, Kapoor A. 2015. Prostate cancer stem cells: deciphering the origins and pathways involved in prostate tumorigenesis and aggression. Oncotarget **6**:1900–1919. DOI: https://doi.org/10.18632/oncotarget.2953, PMID: 25595909

Sekar A, Leiblich A, Wainwright SM, Mendes CC, Sarma D, Hellberg JEEU, Gandy C, Goberdhan DCI, Hamdy FC, Wilson C. 2023. Rbf/E2F1 control growth and endoreplication via steroid-independent Ecdysone Receptor signalling in Drosophila prostate-like secondary cells. PLoS genetics **19**:e1010815. DOI: https://doi.org/10.1371/journal.pgen.1010815, PMID: 37363926

Sharma V, Pandey AK, Kumar A, Misra S, Gupta HPK, Gupta S, Singh A, Buehner NA, Ravi Ram K. 2017. Functional male accessory glands and fertility in Drosophila require novel ecdysone receptor. PLoS genetics **13**:e1006788. DOI: https://doi.org/10.1371/journal.pgen.1006788, PMID: 28493870

Sharp A, Coleman I, Yuan W, Sprenger C, Dolling D, Rodrigues DN, Russo JW, Figueiredo I, Bertan C, Seed G, Riisnaes R, Uo T, Neeb A, Welti J, Morrissey C, Carreira S, Luo J, Nelson PS, Balk SP, True LD, de

838 Bono JS, Plymate SR. 2019. Androgen receptor splice variant-7 expression emerges with castration
839 resistance in prostate cancer. The Journal of clinical investigation **129**:192–208. DOI:
840 https://doi.org/10.1172/JCI122819, PMID: 30334814
841 Shen J, Lu J, Sui L, Wang D, Yin M, Hoffmann I, Legler A, Pflugfelder GO. 2014. The orthologous Tbx
842 transcription factors Omb and TBX2 induce epithelial cell migration and extrusion in vivo without
843 involvement of matrix metalloproteinases. Oncotarget **5**:11998–12015. DOI:
844 https://doi.org/10.18632/oncotarget.2426, PMID: 25344916
845 Shirai T, Sekai M, Kozawa K, Sato N, Tanimura N, Kon S, Matsumoto T, Murakami T, Ito S, Tilston-Lunel A,
846 Varelas X, Fujita Y. 2022. Basal extrusion of single-oncogenic mutant cells induces dome-like
847 structures with altered microenvironments. Cancer science **113**:3710–3721. DOI:
848 https://doi.org/10.1111/cas.15483, PMID: 35816400
849 Slattum G, McGee KM, Rosenblatt J. 2009. P115 RhoGEF and microtubules decide the direction apoptotic cells
850 extrude from an epithelium. The Journal of Cell Biology **186**:693–702. DOI:
851 https://doi.org/10.1083/jcb.200903079, PMID: 19720875
852 Stelloo S, Nevedomskaya E, Kim Y, Schuurman K, Valle-Encinas E, Lobo J, Krijgsman O, Peeper DS, Chang
853 SL, Feng FY-C, Wessels LFA, Henrique R, Jerónimo C, Bergman AM, Zwart W. 2018. Integrative
854 epigenetic taxonomy of primary prostate cancer. Nature communications **9**:4900. DOI:
855 https://doi.org/10.1038/s41467-018-07270-2, PMID: 30464211
856 Suntsova M, Gaifullin N, Allina D, Reshetun A, Li X, Mendeleeva L, Surin V, Sergeeva A, Spirin P, Prassolov
857 V, Morgan A, Garazha A, Sorokin M, Buzdin A. 2019. Atlas of RNA sequencing profiles for normal
858 human tissues. Scientific data **6**:36. DOI: https://doi.org/10.1038/s41597-019-0043-4, PMID: 31015567
859 Taniguchi K, Kokuryo A, Imano T, Nakagoshi H, Adachi-Yamada T. 2018. Binucleation of Accessory Gland
860 Lobe Contributes to Effective Ejection of Seminal Fluid in Drosophila *melanogaster*. Zoological
861 Science **35**:446–458. DOI: https://doi.org/10.2108/zs170188, PMID: 30298781
862 The Genotype-Tissue Expression (GTEx) project. 2013. Nature genetics **45**:580–585. DOI:
863 https://doi.org/10.1038/ng.2653, PMID: 23715323
864 Turpin A, Delliaux C, Parent P, Chevalier H, Escudero-Iriarte C, Bonardi F, Vanpouille N, Flourens A, Querol J,
865 Carnot A, Leroy X, Herranz N, Lanel T, Villers A, Olivier J, Touzet H, de Launoit Y, Tian TV,
866 Duterque-Coquillaud M. 2023. Fascin-1 expression is associated with neuroendocrine prostate cancer
867 and directly suppressed by androgen receptor. British Journal of Cancer **129**:1903–1914. DOI:
868 https://doi.org/10.1038/s41416-023-02449-x
869 Ventrella R, Kim SK, Sheridan J, Grata A, Bresteau E, Hassan OA, Suva EE, Walentek P, Mitchell BJ. 2023.
870 Bidirectional multiciliated cell extrusion is controlled by Notch-driven basal extrusion and Piezo1-
871 driven apical extrusion. Development (Cambridge, England) **150**:dev201612. DOI:
872 https://doi.org/10.1242/dev.201612, PMID: 37602491
873 Vialat M, Baabdaty E, Trousson A, Kocer A, Lobaccaro J-MA, Baron S, Morel L, de Joussineau C. 2024.
874 Cholesterol Dietary Intake and Tumor Cell Homeostasis Drive Early Epithelial Tumorigenesis: A
875 Potential Modelization of Early Prostate Tumorigenesis. Cancers **16**. DOI:
876 https://doi.org/10.3390/cancers16112153, PMID: 38893271
877 Villeneuve C, Lagoutte E, de Plater L, Mathieu S, Manneville J-B, Maître J-L, Chavrier P, Rossé C. 2019.
878 aPKCi triggers basal extrusion of luminal mammary epithelial cells by tuning contractility and vinculin
879 localization at cell junctions. Proceedings of the National Academy of Sciences of the United States of
880 America **116**:24108–24114. DOI: https://doi.org/10.1073/pnas.1906779116, PMID: 31699818
881 Wilson C, Leiblich A, Goberdhan DCI, Hamdy F. 2017. The Drosophila Accessory Gland as a Model for
882 Prostate Cancer and Other Pathologies. *Current Topics in Developmental Biology*. p. 339–375. DOI:
883 https://doi.org/10.1016/bs.ctdb.2016.06.001, PMID: 28057306
884 Wu HC, Hsieh JT, Gleave ME, Brown NM, Pathak S, Chung LW. 1994. Derivation of androgen-independent
885 human LNCaP prostatic cancer cell sublines: role of bone stromal cells. International journal of cancer
886 **57**:406–412. DOI: https://doi.org/10.1002/ijc.2910570319, PMID: 8169003
887 Xue L, Noll M. 2002. Dual role of the Pax gene paired in accessory gland development of Drosophila.
888 Development (Cambridge, England) **129**:339–46. PMID: 11807027
889 Zhao J, Sun G, Zhu S, Dai J, Chen J, Zhang M, Ni Y, Zhang H, Shen P, Zhao X, Zhang B, Pan X, Nie L, Yin X,
890 Liang J, Zhang X, Wang Z, Zhu X, Liao B, Liu Z, Armstrong CM, Gao AC, Huang H, Chen N, Zeng
891 H, Porter LH, Hashimoto K, Lawrence MG, Pezaro C, Clouston D, Wang H, Papargiris M, Thorne H,
892 Li J, Ryan A, Norden S, Moon D, Bolton DM, Sengupta S, Frydenberg M, Murphy DG, Risbridger GP,
893 Taylor RA, Bonkhoff H, Wheeler TM, van der Kwast TH, Magi-Galluzzi C, Montironi R, Cohen RJ.
894 2018. Intraductal carcinoma of the prostate: precursor or aggressive phenotype of prostate cancer? BJU
895 international **121**:971–978. DOI: https://doi.org/10.1002/pros.22579, PMID: 28977728

896 Zhou J-R, Yu L, Zerbini LF, Libermann TA, Blackburn GL. 2004. Progression to androgen-independent LNCaP
897 human prostate tumors: cellular and molecular alterations. International journal of cancer **110**:800–806.
898 DOI: https://doi.org/10.1002/ijc.20206, PMID: 15170660
899 Zoeller JJ, Bronson RT, Selfors LM, Mills GB, Brugge JS. 2017. Niche-localized tumor cells are protected from
900 HER2-targeted therapy via upregulation of an anti-apoptotic program in vivo. NPJ breast cancer **3**:18.
901 DOI: https://doi.org/10.1038/s41523-017-0020-z, PMID: 28649658
902 Zundelevich A, Dadiani M, Kahana-Edwin S, Itay A, Sella T, Gadot M, Cesarkas K, Farage-Barhom S, Saar EG,
903 Eyal E, Kol N, Pavlovski A, Balint-Lahat N, Dick-Necula D, Barshack I, Kaufman B, Gal-Yam EN.
904 2020. ESR1 mutations are frequent in newly diagnosed metastatic and loco-regional recurrence of
905 endocrine-treated breast cancer and carry worse prognosis. Breast cancer research : BCR **22**:16. DOI:
906 https://doi.org/10.1186/s13058-020-1246-5, PMID: 32014063
907
908

909 **Fig. 1. Androgen signaling activity negatively correlates with prostate cancer**
910 **progression.**
911 (A-B) mRNA expression in normal (green), primary (red) or castration-resistant (CRPC)
912 prostate cancer samples. (A) *AR* expression. (B) *AR* target genes expression. (C) Principal
913 component analysis of sample expression defines a trajectory of disease progression with an
914 associated pseudotime score (extracted from Prostate Cancer Atlas). (D) Pseudotime
915 correlation segregates normal, primary, CRPC and neuroendocrine (NEPC) samples. (E)
916 Individual *AR* expression in the samples along the trajectory. (F) Relative change of
917 expression of AR during progression. X-axis represents Pearson's correlation coefficient
918 between mRNAs and pseudotime as Y-axis displays the associated significance adjusted for
919 false discovery rate (FDR). (G) Individual *AR* expression in the samples depending on
920 pseudotime (X-axis) and sample type (color code). (H) CRPC samples are separated in four
921 quartiles (1ST to 4TH QT) depending on their pseudotime. *AR* expression is then plotted for
922 individual samples. (I-N) Individual expression and relative change of expression of three AR
923 target genes (SPOP, KLK3, NKX3-1) during progression. * $p<0.05$; ** $p<0.01$;
924 ****$p<0.0001$.

925 **Fig. 2. Loss of correlation between AR expression and canonical AR signaling coincides**
926 **with downregulated expression of *SRD5A2*.**
927 (A) Individual *AR* expression (X-axis) versus ALDHIA3 expression (Y-axis) in the samples
928 depending on sample type (color code). (B-D) Same expression separated by sample type. (E)
929 *SRD5A2* -coding for the DHT-producing enzyme- mRNA expression in normal (green),
930 primary (red) or castration-resistant (CRPC) prostate cancer samples. (F-G) Individual
931 expression and relative change of expression of *SRD5A2* during progression. (H) Primary
932 samples are separated in four quartiles (1ST to 4TH QT) depending on their pseudotime.
933 *SRD5A2* expression is then plotted for individual samples. ****$p<0.0001$.

934 **Fig. 3. Treatment-like effect induced by Ecdysone Receptor downregulation**

935 (A-L and R-U) Confocal imaging of accessory glands (delimited by white dashes). White
936 arrowheads indicate epithelial clones. Empty arrowheads indicate extra-epithelial tumors.
937 Yellow arrowheads indicate a tumor cell population specific to EGFRλ EcR-KD genotype.
938 (A-D) FISH detection of EcR mRNA in EGFRλ CTL and EGFRλ EcR-KD genotypes. (E-L)
939 Shared phenotypes between the two genotypes. (M-O) Extra-epithelial tumor characteristics
940 defined by 3D-reconstruction. (P) % of glands bearing extra-epithelial tumors 4, 5 or 6 days
941 after clonal induction for the different genotypes. (Q) Comparison of the maximal extra-
942 epithelial tumors percentage (at 6D) between the two genotypes. (R-U) Cleaved caspase 3
943 staining in the different tumor cell populations. (V) Quantification of the number of apoptotic
944 extra-epithelial tumors at 5, 6 or 10 days after clonal induction for the different genotypes.
945 Scale bars: 50µm. Number of experiments (N) and of individual flies (n) are given in Table 2.
946 Statistical tests are explained in the Methods section; ns: non-significant; * $p<0.05$; **
947 $p<0.01$; *** $p<0.001$; ****$p<0.0001$.

948 **Fig. 4. Tumor escape induced by Ecdysone Receptor downregulation.**

949 (A-T) Confocal imaging of accessory glands (delimited by white dashes in some images).
950 White arrowheads indicate epithelial clones. Empty arrowheads indicate extra-epithelial
951 tumors. Yellow arrowheads indicate the new tumor cell population which is specific to
952 EGFRλ EcR-KD genotype. (A-D) Coracle staining indicates epithelial status of the cells. (E-
953 H) Cleaved caspase 3 staining in the different tumor cell populations 10 days after clonal
954 induction for the different genotypes. (I-L) Phospho-Histone 3 staining 6 days after clonal
955 induction for the different genotypes. (M-P) Phospho-Src staining 6 days after clonal
956 induction for the different genotypes. (Q-R) DAPI staining reveals nuclear shapes of cells of
957 the new population (yellow empty arrowheads). (S-T) Multiple axes of growth (double-

958 headed arrows) and F-actin reorganization (phalloidin staining, magenta) in the new tumor
959 cell population. Scale bars: 50µm.

960 **Fig. 5. Basal extrusion is modified in case of tumor escape.**
961 (A-T) Confocal imaging of accessory glands. White arrowheads indicate epithelial clones.
962 Empty arrowheads indicate extra-epithelial tumors. Yellow arrowheads indicate the new
963 tumor cell population which is specific to EGFRλ EcR-KD genotype. (A-B, E-F) XYZ
964 imaging. Glands are delimited by white dashes in B and F. (C-D, G-H) XZY orthogonal
965 reconstructions of the glands, showing the lumens and in-depth view of the epithelium.
966 Epithelium pushed into the lumen is delimited by white dashes in G and H, as intrabasal
967 tumor cells lay between this epithelium and the basement membrane (yellow). (I) % of glands
968 bearing intrabasal tumors 6 or 7 days after clonal induction for the different genotypes. (J-L)
969 Comparison of intrabasal vs other tumor characteristics defined by 3D-reconstruction (C:
970 clones; T: extra-epithelial tumors; IB-T: intrabasal tumors). Scale bars: 50µm in XYZ views
971 and 20µm in XZY reconstructions. ns: non-significant; ** $p<0.01$; *** $p<0.001$;
972 ****$p<0.0001$.

973 **Fig. 6. Ecdysone-dependent molecular control of tumor escape and basal extrusion.**
974 (A-B) % of glands bearing extra-epithelial (A) or intrabasal tumors (B) 6 days after clonal
975 induction for different genotypes. (C-D') Confocal imaging of accessory glands. Yellow
976 arrowheads indicate intrabasal tumors. (C, D) XYZ imaging. (C', D') Corresponding XZY
977 orthogonal reconstructions of the glands, showing the lumens and in-depth view of the
978 epithelium. Epithelium pushed into the lumen is delimited by white dashes. (E-H) β3 Tubulin
979 staining 6 days after clonal induction for different genotypes. Glands are delimited by white
980 dashes, white arrowheads indicate tumors clones. (I-I') Confocal imaging of accessory glands.
981 (I) XYZ imaging. (I') Corresponding XZY orthogonal reconstruction of the glands. (J) % of
982 glands bearing extra-epithelial (left) or intrabasal tumors (right) 6 days after clonal induction

983 for different genotypes. (K) Comparison of proliferation rates defined by 3D-reconstruction

984 (E: epithelial clones; IB-T: intrabasal tumors; IB: intrabasal cells in EGFRλ Tub60D-KD

985 genotype). Scale bars: 50µm in XYZ views and 20µm in XZY reconstructions. ** $p<0.01$;

986 *** $p<0.001$; ****$p<0.0001$.

987

988 **Table 1. Canonical AR Signaling genes are downregulated in CRPC compared with**

989 **primary cancer.**

990 Based on 173 Normal samples, 708 Primary cancer samples and 484 CRPC samples. In

991 yellow: six of the genes are significantly less expressed in CRPC than in normal samples.

	p values			Median ± standard deviation			Mean values ± STD error		
Gene	Normal vs primary	Normal vs CRPC	Primary vs CRPC	Normal	Primary	CRPC	Normal	Primary	CRPC
AR	<0,0001	<0,0001	<0,0001	6.933 ± 0.8056	7.419 ± 0.636	9.929 ± 3.374	6,784 ± 0.06125	7,418 ± 0.0239	9,056 ± 0.1534
ABCC4	<0,0001	0.0367	<0,0001	5.939 ± 1.381	8.991 ± 1.157	5.58 ±2.3	6,06 ± 0.105	8,857 ± 0.04349	5,697 ± 0.1045
ALDH1A3	<0,0001	<0,0001	<0,0001	7.666 ± 1.005	9.068 ± 0.9679	5.825 ± 1.97	7,571 ± 0.07643	8,976 ± 0.03638	5,746 ± 0.08956
AMACR	<0,0001	<0,0001	<0,0001	4.061 ± 1.233	8.642 ± 1.752	7.152 ± 2.431	4,252 ± 0.09375	8,437 ± 0.06586	7,239 ± 0.1105
CAMKK2	<0,0001	<0,0001	<0,0001	6.477 ± 0.6324	7.967± 0.9343	6.828 ± 1.175	6,511 ± 0.04808	7,966 ± 0.03511	6,958 ± 0.0534
FASN	<0,0001	<0,0001	<0,0001	8.332 ± 1.229	9.804 ± 1.181	9.121 ± 1.91	8,539 ± 0.0934	9,742 ± 0.04437	9,112 ± 0.08681
KLK2	<0,0001	<0,0001	<0,0001	11.65 ± 2.982	12.35 ± 0.8887	10.67 ± 3.741	10,7 ± 0.2267	12,21 ± 0.0334	9,458 ± 0.17
KLK3	<0,0001	<0,0001	<0,0001	12.65 ± 3.081	13.87 ± 0.9249	11.69 ± 3.875	11,66 ± 0.2342	13,73 ± 0.03476	10,16 ± 0.1761
NKX3-1	<0,0001	0.2104	<0,0001	8.926 ± 2.264	10.1 ± 0.5656	9.003 ± 2.935	8,021 ± 0.1721	10,05 ± 0.02126	7,975 ± 0.1334
PART1	<0,0001	0.0171	<0,0001	5.019 ± 1.467	6.068 ± 1.04	4.5 ± 2.111	4,744 ± 0.1116	5,956 ± 0.03909	4,267 ± 0 09594
PCA3	<0,0001	0.3735	<0,0001	1.54 ± 1.944	7.868 ± 2.568	2.132 ± 3.014	2,2 ± 0.1402	7,154 ± 0.09653	3,049 ± 0.137
PLPP1	<0,0001	0.1708	<0,0001	8.018 ± 1.084	8.733 ± 0.8458	8.283 ± 1.855	7,94 ± 0.08239	8,702 ± 0.03179	7,903 ± 0.08431
PMEPA1	<0,0001	0.0363	<0,0001	7.931 ± 1.239	9.483 ± 0.6337	8.428 ± 1.874	7,879 ± 0.09418	9,393 ± 0.02382	7,996 ± 0.08516
STEAP1	<0,0001	<0,0001	<0,0001	5.077 ± 1.43	7.043 ± 0.7164	6.638 ± 2.178	5,032 ± 0.1087	6,968 ± 0.02692	6,041 ± 0.09901
STEAP2	<0,0001	0.059	<0,0001	8.058 ± 1.332	9.376 ± 0.8335	8.436 ± 2.767	7,867 ± 0.1013	9,276 ± 0.03132	7,709 ± 0.1258
STEAP4	<0,0001	0.0416	<0,0001	7.036 ± 1.186	8.596 ± 1.178	6.728 ± 2.371	7,045 ± 0.09017	8,486 ± 0.04429	6,581 ± 0.1078

992

993 **Table 2. Numbers of independent experiments (N) and individuals (n) used in the**
994 **different experiments.**

995

Figure panel	N = Number of independent experiments	n = total number of individuals
Fig. 1 and 2	N = 13 independent cohorts	n = 1140
Fig. 3M-O	EGFRλ CTL: 6; EGFRλ EcR-KD: 8	EGFRλ CTL: 29; EGFRλ EcR-KD: 35
Fig. 3P	for respective column: 4, 3, 30, 4, 3, 36	for respective column: 60, 131, 1144, 217, 123, 1525
Fig. 3Q	EGFRλ CTL: 30; EGFRλ EcR-KD: 36	EGFRλ CTL: 1144 EGFRλ EcR-KD: 1525
Fig. 3V	3	for respective column : 32, 36, 7, 17, 22, 25
Fig. 5I	3	for respective column: 203, 196, 217, 268
Fig. 5J-L	3	for respective column of each panel: 53, 35, 30
Fig. 6A	For respective column, 30, 36, 7, 9, 8, 33, 12.	For respective column: 1144, 1525, 228, 287, 207, 1618, 637.
Fig. 6B	N = 3 for all columns	For respective column: 203, 217, 52, 126, 62, 252, 167.
Fig. 6J	Left panel: 30, 14; right panel: 3 or more	Left panel: 1576, 354; right panel: 248, 130
Fig. 6K	3 or more	for respective column: 51, 30, 25

996

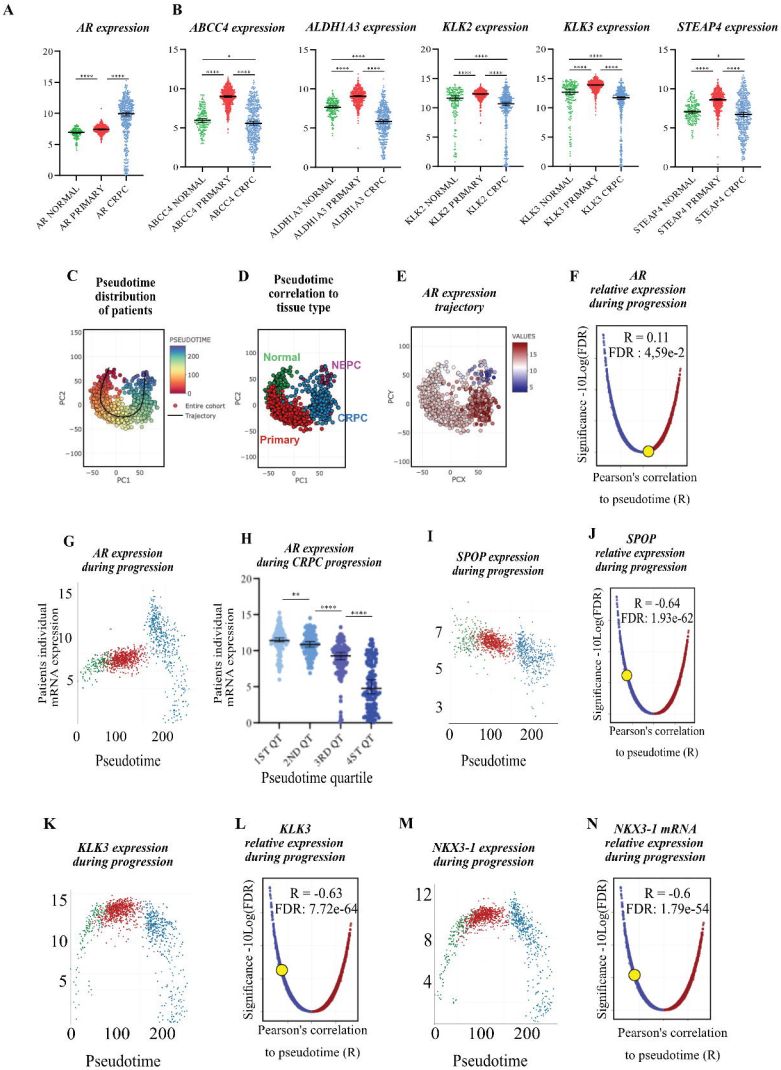
A
AR expression
AR NORMAL
AR PRIMARY
AR CRPC
B
ABCC4 expression
ABCC4 NORMAL
ABCC4 PRIMARY
ABCC4 CRPC
ALDH1A3 expression
ALDH1A3 NORMAL
ALDH1A3 PRIMARY
ALDH1A3 CRPC
KLK2 expression
KLK2 NORMAL
KLK2 PRIMARY
KLK2 CRPC
KLK3 expression
KLK3 NORMAL
KLK3 PRIMARY
KLK3 CRPC
STEAP4 expression
STEAP4 NORMAL
STEAP4 PRIMARY
STEAP4 CRPC
C
Pseudotime distribution of patients
PSEUDOTIME
Entire cohort
Trajectory
PC1
PC2
D
Pseudotime correlation to tissue type
Normal
NEPC
CRPC
Primary
E
AR expression trajectory
VALUES
PCX
PCY
F
AR relative expression during progression
R = 0.11
FDR : 4,59e-2
Significance -10Log(FDR)
Pearson's correlation to pseudotime (R)
G
AR expression during progression
Patients individual mRNA expression
Pseudotime
H
AR expression during CRPC progression
Patients individual mRNA expression
1ST QT
2ND QT
3RD QT
4ST QT
Pseudotime quartile
I
SPOP expression during progression
Pseudotime
J
SPOP relative expression during progression
R = -0.64
FDR: 1.93e-62
Significance -10Log(FDR)
Pearson's correlation to pseudotime (R)
K
KLK3 expression during progression
Pseudotime
L
KLK3 relative expression during progression
R = -0.63
FDR: 7.72e-64
Significance -10Log(FDR)
Pearson's correlation to pseudotime (R)
M
NKX3-1 expression during progression
Pseudotime
N
NKX3-1 mRNA relative expression during progression
R = -0.6
FDR: 1.79e-54
Significance -10Log(FDR)
Pearson's correlation to pseudotime (R)

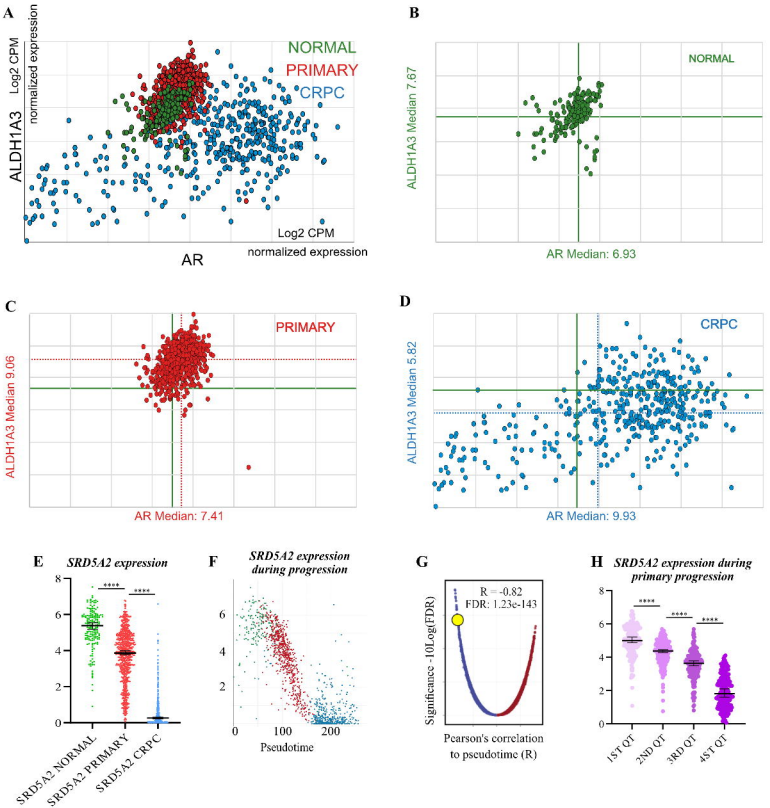
A
NORMAL
PRIMARY
CRPC
ALDH1A3 Log2 CPM normalized expression
AR Log2 CPM normalized expression
B
NORMAL
ALDH1A3 Median 7.67
AR Median: 6.93
C
PRIMARY
ALDH1A3 Median 9.06
AR Median: 7.41
D
CRPC
ALDH1A3 Median 5.82
AR Median: 9.93
E
SRD5A2 expression
****
****
SRD5A2 NORMAL
SRD5A2 PRIMARY
SRD5A2 CRPC
F
SRD5A2 expression during progression
Pseudotime
G
R = -0.82
FDR: 1.23e-143
Significance -10Log(FDR)
Pearson's correlation to pseudotime (R)
H
SRD5A2 expression during primary progression
****
****
****
1ST QT
2ND QT
3RD QT
4ST QT

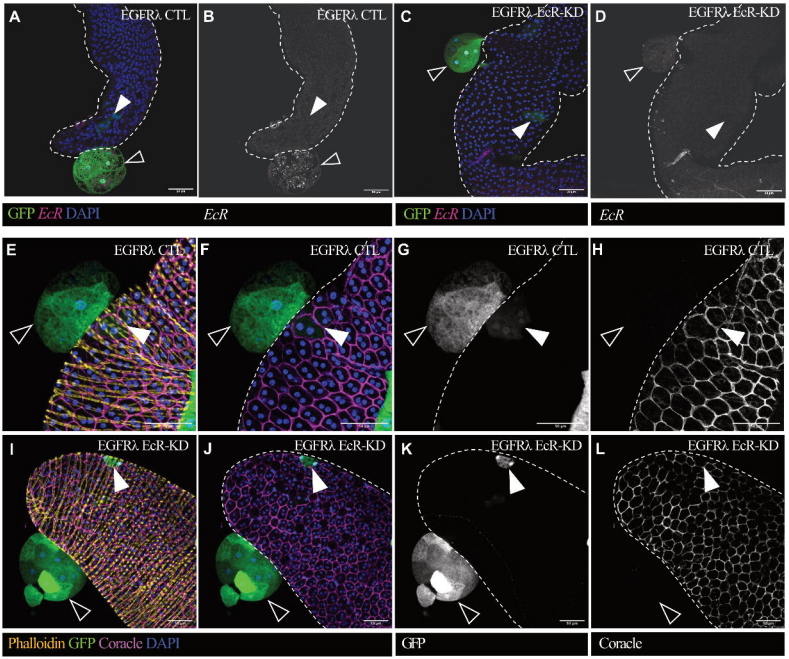
A
EGFRλ CTL
B
EGFRλ CTL
C
EGFRλ EcR-KD
D
EGFRλ EcR-KD
GFP EcR DAPI
EcR
GFP EcR DAPI
EcR
E
EGFRλ CTL
F
EGFRλ CTL
G
EGFRλ CTL
H
EGFRλ CTL
I
EGFRλ EcR-KD
J
EGFRλ EcR-KD
K
EGFRλ EcR-KD
L
EGFRλ EcR-KD
Phalloidin GFP Coracle DAPI
GFP
Coracle

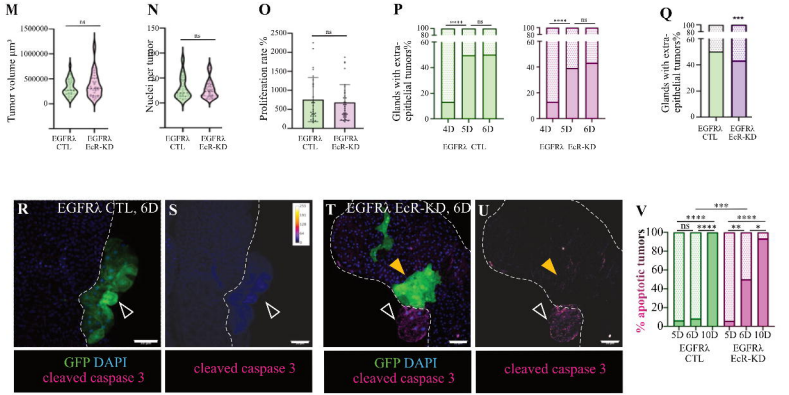
M
Tumor volume µm³
1500000
1000000
500000
0
ns
EGFRλ CTL
EGFRλ EcR-KD
N
Nuclei per tumor
150
100
50
0
ns
EGFRλ CTL
EGFRλ EcR-KD
O
Proliferation rate %
2500
2000
1500
1000
500
0
ns
EGFRλ CTL
EGFRλ EcR-KD
P
Glands with extra-epithelial tumors%
100
80
60
40
20
0
****
ns
4D
5D
6D
EGFRλ CTL
****
ns
4D
5D
6D
EGFRλ EcR-KD
Q
Glands with extra-epithelial tumors%
100
80
60
40
20
0
***
EGFRλ CTL
EGFRλ EcR-KD
R
EGFRλ CTL, 6D
S
T
EGFRλ EcR-KD, 6D
U
GFP DAPI
cleaved caspase 3
cleaved caspase 3
GFP DAPI
cleaved caspase 3
cleaved caspase 3
V
% apoptotic tumors
100
80
60
40
20
0
***
****
ns
****
**
*
5D
6D
10D
5D
6D
10D
EGFRλ CTL
EGFRλ EcR-KD

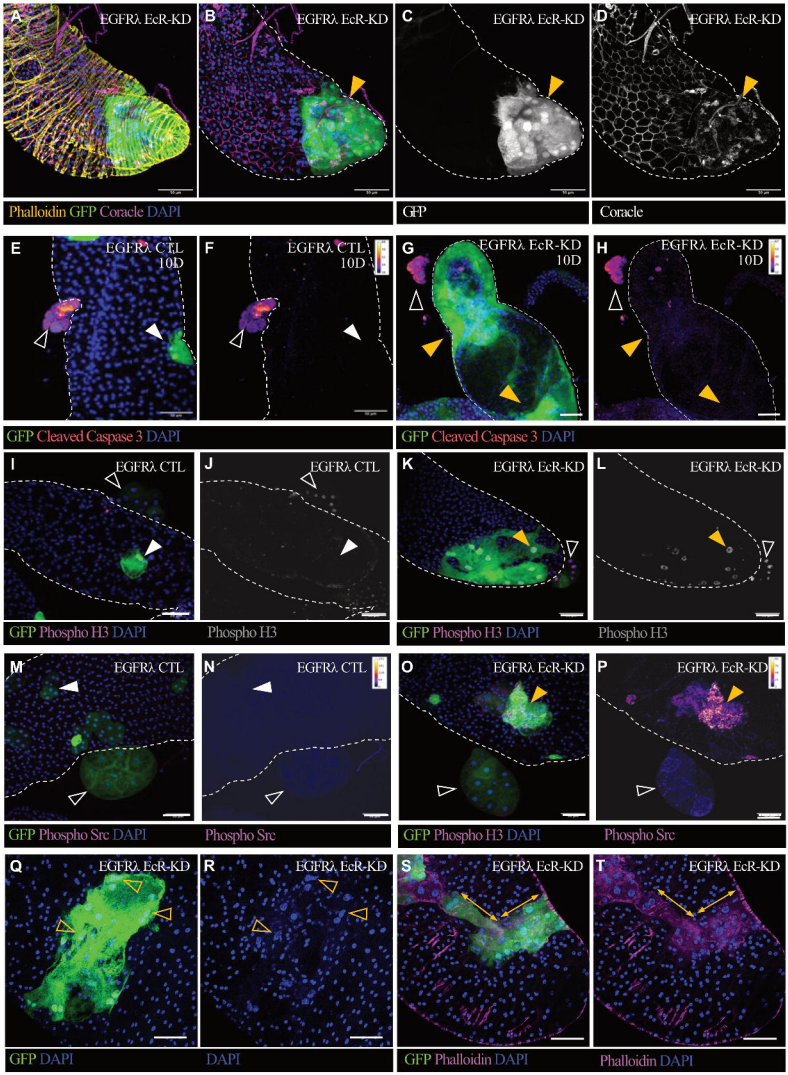
A
EGFRλ EcR-KD
B
EGFRλ EcR-KD
C
EGFRλ EcR-KD
D
EGFRλ EcR-KD
Phalloidin GFP Coracle DAPI
GFP
Coracle
E
EGFRλ CTL
10D
F
EGFRλ CTL
10D
G
EGFRλ EcR-KD
10D
H
EGFRλ EcR-KD
10D
GFP Cleaved Caspase 3 DAPI
GFP Cleaved Caspase 3 DAPI
I
EGFRλ CTL
J
EGFRλ CTL
K
EGFRλ EcR-KD
L
EGFRλ EcR-KD
GFP Phospho H3 DAPI
Phospho H3
GFP Phospho H3 DAPI
Phospho H3
M
EGFRλ CTL
N
EGFRλ CTL
O
EGFRλ EcR-KD
P
EGFRλ EcR-KD
GFP Phospho Src DAPI
Phospho Src
GFP Phospho H3 DAPI
Phospho Src
Q
EGFRλ EcR-KD
R
EGFRλ EcR-KD
S
EGFRλ EcR-KD
T
EGFRλ EcR-KD
GFP DAPI
DAPI
GFP Phalloidin DAPI
Phalloidin DAPI

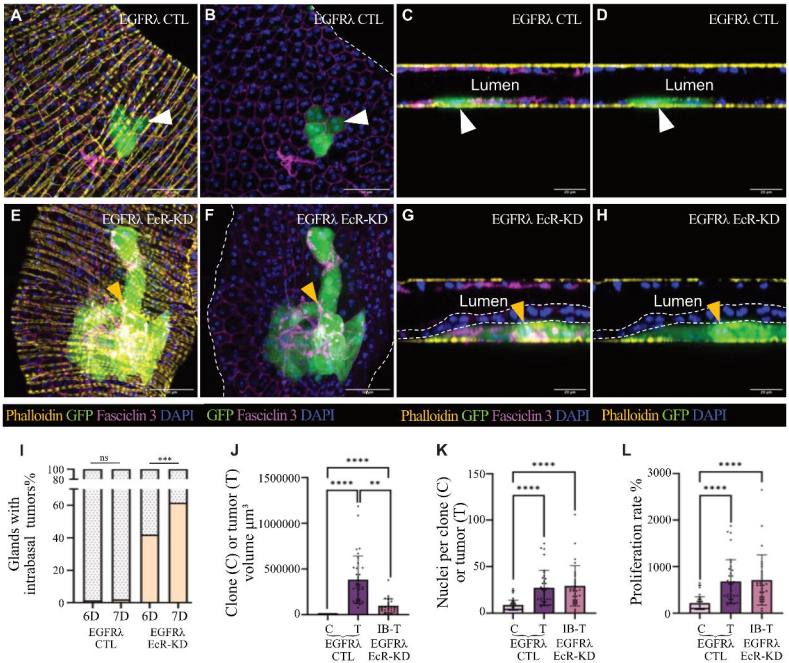
A
EGFRλ CTL
B
EGFRλ CTL
C
EGFRλ CTL
Lumen
D
EGFRλ CTL
Lumen
E
EGFRλ EcR-KD
F
EGFRλ EcR-KD
G
EGFRλ EcR-KD
Lumen
H
EGFRλ EcR-KD
Lumen
Phalloidin GFP Fasciclin 3 DAPI
GFP Fasciclin 3 DAPI
Phalloidin GFP Fasciclin 3 DAPI
Phalloidin GFP DAPI
I
Glands with intrabasal tumors%
ns
***
6D
7D
6D
7D
EGFRλ CTL
EGFRλ EcR-KD
J
Clone (C) or tumor (T) volume µm³
****
****
**
C
T
IB-T
EGFRλ CTL
EGFRλ EcR-KD
K
Nuclei per clone (C) or tumor (T)
****
****
C
T
IB-T
EGFRλ CTL
EGFRλ EcR-KD
L
Proliferation rate %
****
****
C
T
IB-T
EGFRλ CTL
EGFRλ EcR-KD

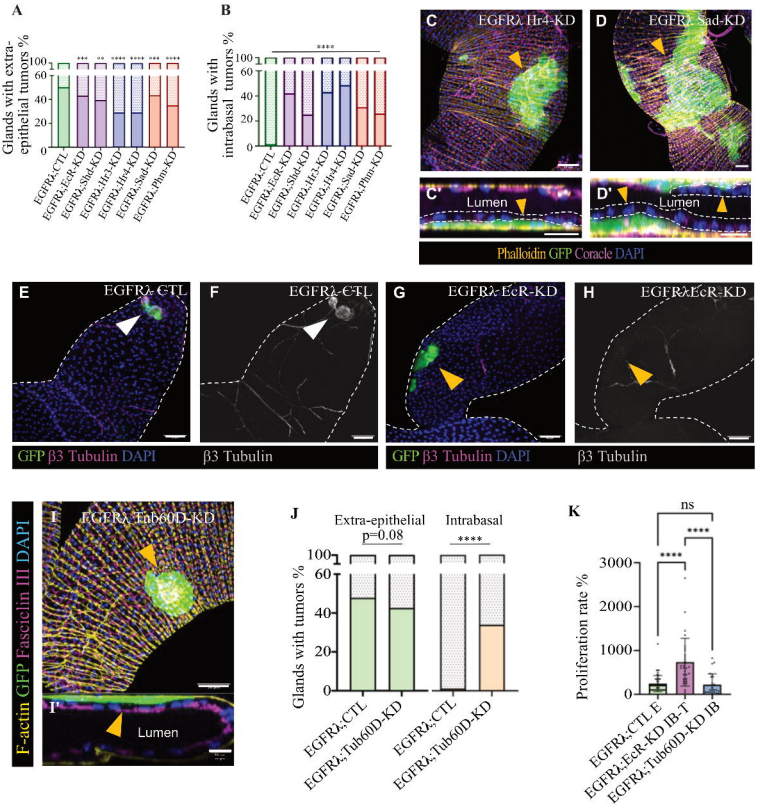
A
Glands with extra-epithelial tumors %
100
60
40
20
0
***
**
****
****
***
****
EGFRλ-CTL
EGFRλ-EcR-KD
EGFRλ-Shd-KD
EGFRλ-Hr3-KD
EGFRλ-Hr4-KD
EGFRλ-Sad-KD
EGFRλ-Phn-KD
B
Glands with intrabasal tumors %
****
C
EGFRλ-Hr4-KD
D
EGFRλ-Sad-KD
C'
Lumen
D'
Lumen
Phalloidin GFP Coracle DAPI
E
EGFRλ-CTL
F
EGFRλ-CTL
G
EGFRλ-EcR-KD
H
EGFRλ-EcR-KD
GFP β3 Tubulin DAPI
β3 Tubulin
GFP β3 Tubulin DAPI
β3 Tubulin
I
EGFRλ-Tub60D-KD
I'
Lumen
F-actin GFP Fasciclin III DAPI
J
Extra-epithelial
p=0.08
Intrabasal
****
Glands with tumors %
EGFRλ-CTL
EGFRλ-Tub60D-KD
EGFRλ-CTL
EGFRλ-Tub60D-KD
K
ns
****
****
Proliferation rate %
3000
2000
1000
0
EGFRλ-CTL E
EGFRλ-EcR-KD IB-T
EGFRλ-Tub60D-KD IB

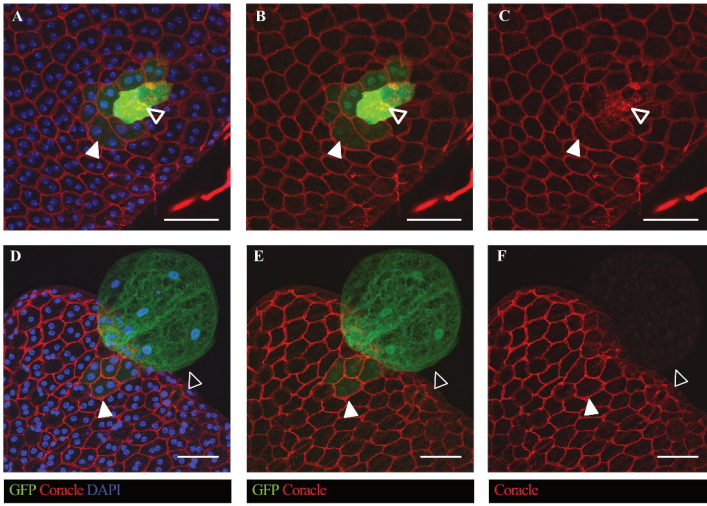

Figure S1: EGFRλ clonal expression induces tumorigenesis in the drosophila accessory gland
White arrowheads: mildly hyperproliferative, hypertrophic cells are well integrated into the epithelium with undisturbed cell-cell interaction (A-F, Coracle staining).
Thick empty arrowheads: some of these epithelial tumor cells express higher levels of GFP (A-B), reflecting modified gene expression, and higher levels of epithelial markers. However, these markers do not properly localize at the membrane (C), indicating a loss of cohesion with neighbor cells.
Empty arrowheads: some tumor cells are able to undergo epithelial basal extrusion to form extra-epithelial tumors. These cells are devoid of epithelial markers, indicating a change in their fate (F).
Scale bars: 50 micrometers.

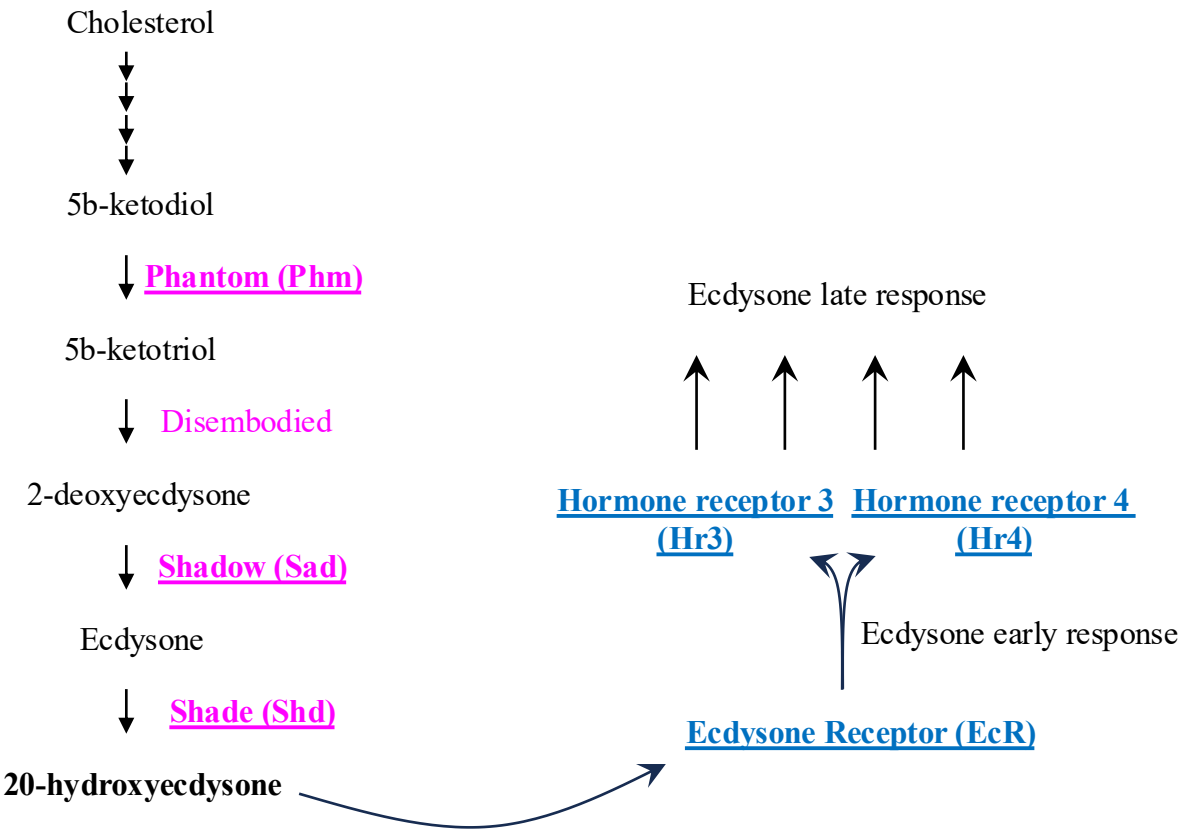

Figure S2: Schematic representation of the late steps of ecdysone synthesis and canonical Ecdysone Signaling.
Six different genes (underlined) were independently targeted by RNAi to block tumor cell production of ecdysone (**Phm, Sad**), metabolization of active 20-hydroxyecdysone (**Shd**), or EcR Signaling (**EcR, Hr3, Hr4**). Results are shown in Fig. 6.

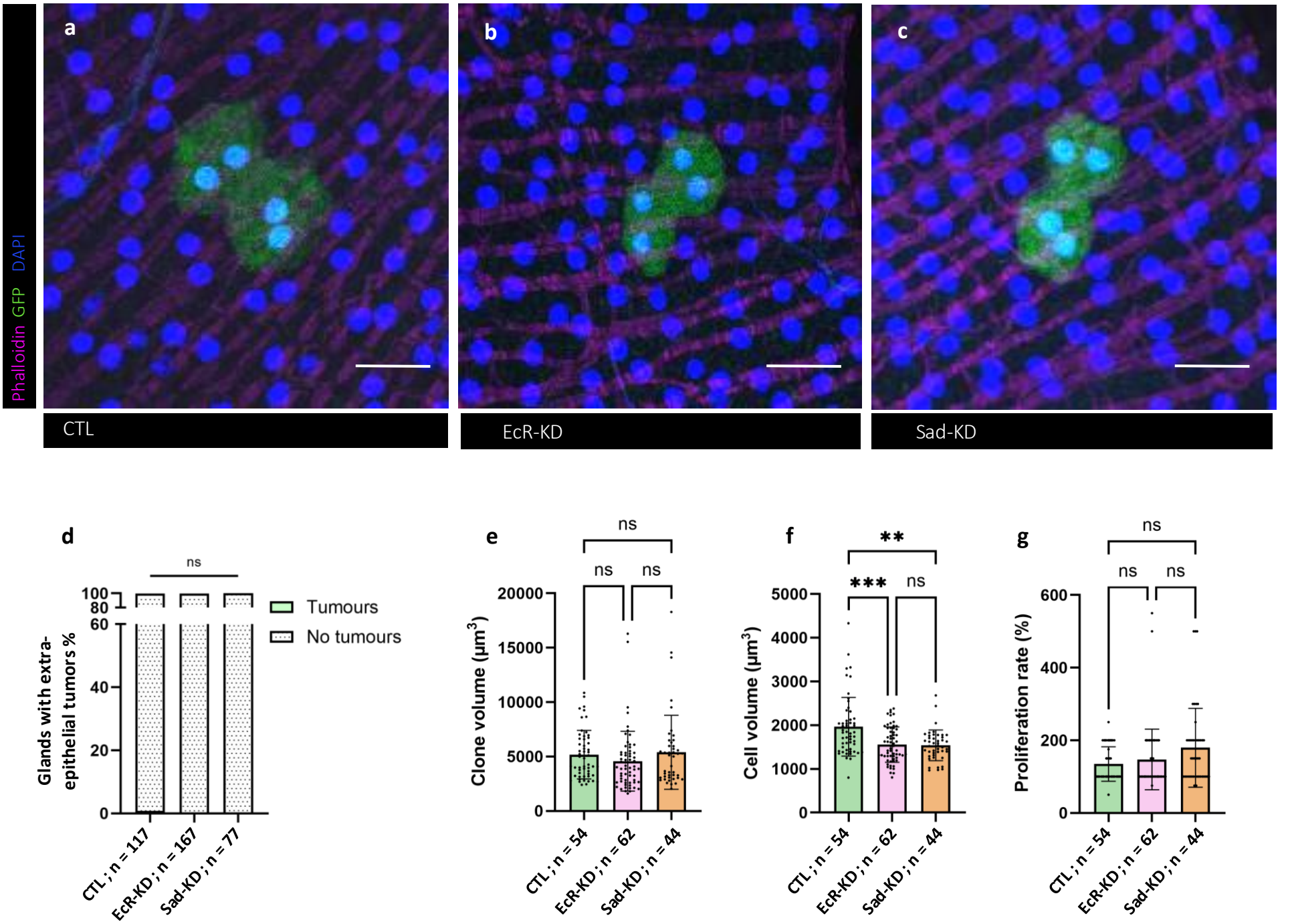

Figure S3 – Ecdsyone deprivation does not promote tumorigenesis by itself.
(a-c) In the absence of expression of an oncogene (CTL), clonal induction of NLS-GFP (a) EcR RNAi (b) or Sad RNAi (c) brings no evident phenotype to the clonal cells. (d) It does not promote tumorigenesis. (e-g) In the absence of average clone volume (e) or difference in proliferation rate compared to control (g), the only noticeable phenotype is a slightly decreased cell size in clones expressing EcR or Sad RNAi (f). Chi^2 test; $^{**}P < 0.01$; $^{***}P < 0.001$. Representative images in (a-c) from three or more experiments. Scale bars: 20 µm.

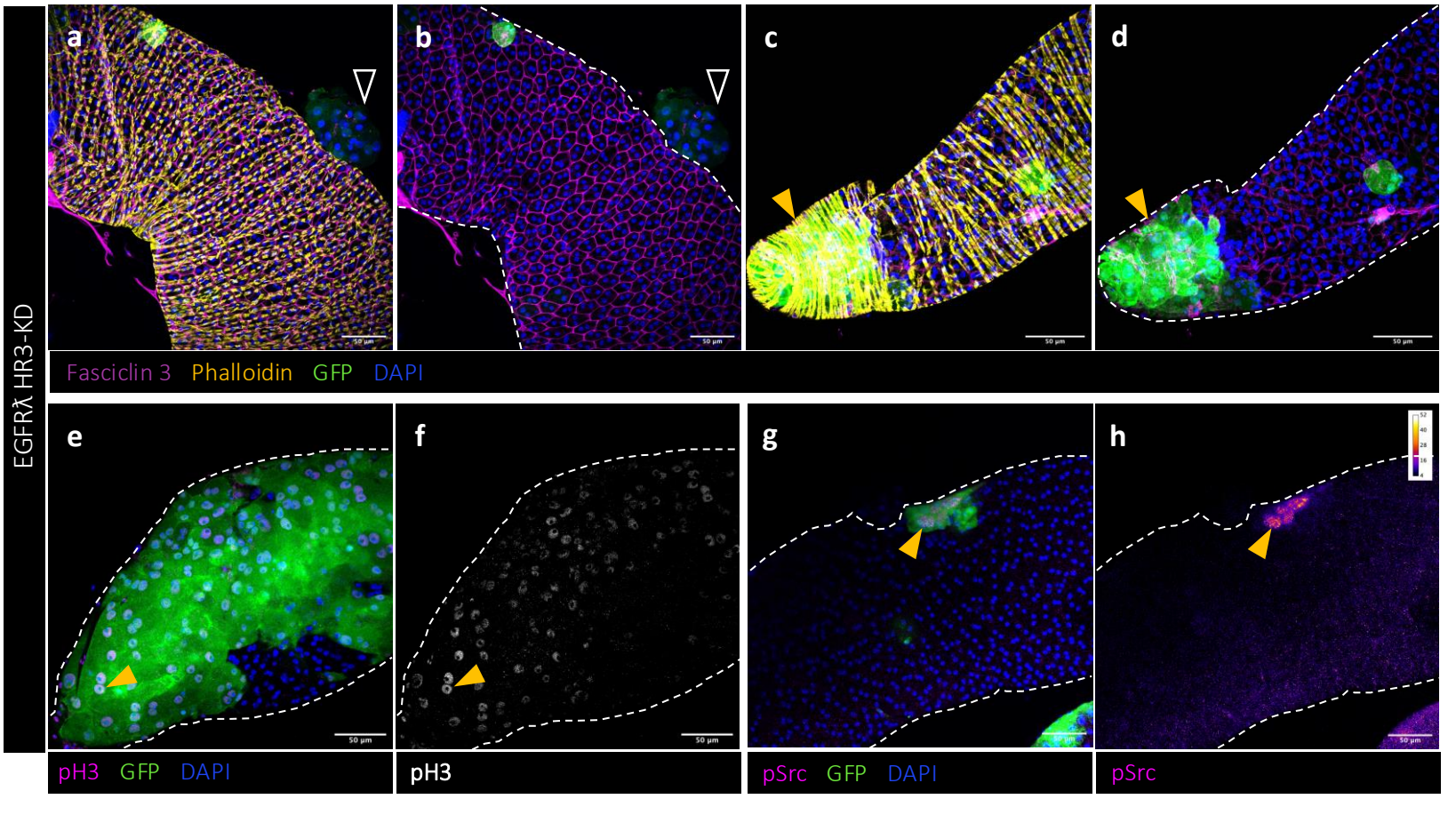

Figure S4 - Downregulation of canonical Ecdysone Signaling induces intrabasal tumorigenesis.
(a-d) Co-expression of Hr3 RNAi suppresses only partially extra-glandular tumors (empty arrowheads in (a-b)) but leads to the appearance of highly proliferative, intrabasal tumor cells into the glands (yellow arrowheads in (c-d)). (e-h) This new population displays a strong staining for classical aggressiveness markers (yellow arrowheads, pH3 staining in (e-f) and pSrc staining in (g-h)). Representative images from three or more experiments. Scale bars: 50 µM.

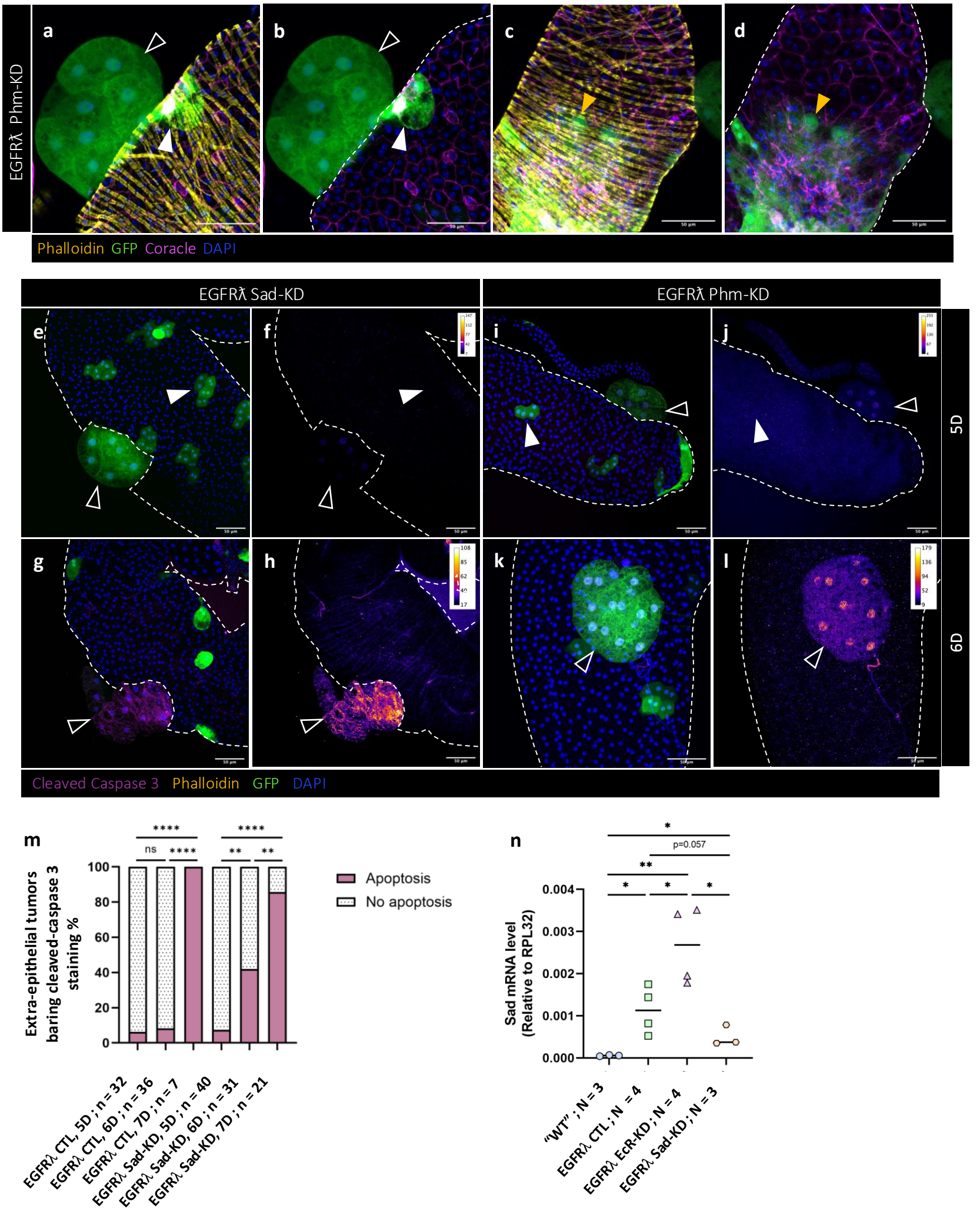

Figure S5 – Loss of autocrine Ecdysone Signaling induces the same paradoxical response as loss of other members of the same pathway.

(a-d) Co-expression of Phm RNAi suppresses only partially the formation of extra-epithelial tumors (empty arrowheads in (a-b)) but leads to the appearance of highly proliferative intrabasal tumors (yellow arrowheads in (c-d)). (e-l) Co-expression of Sad (RNAi (e-h) or Phm RNAi (i-l) induces early apoptosis of extra-epithelial tumors (at 6D, cleaved-caspase 3 staining), mimicking initial effect of steroid deprivation on human tumors (empty arrowheads). (m) Quantification of this early apoptosis phenomenon appearing at 6D for the co-expression of Sad RNAi. (n) qPCR quantification of whole glands expression of Sad for the given genotypes. "WT": glands baring the EGFRλ genetic background, but unable to produce clones, i.e. "wild type" glands. Compared to these, oncogene induction (column 2) induces a significant overexpression of Sad mRNA; co-expression of EcR RNAi (column 3) still significantly increases Sad mRNA expression. Compared to this condition, co-expression of Sad RNAi (column 4) significantly decreases Sad mRNA expression, as expected. Representative images in (a-l) from three or more experiments. Scale bars: 50 µM.

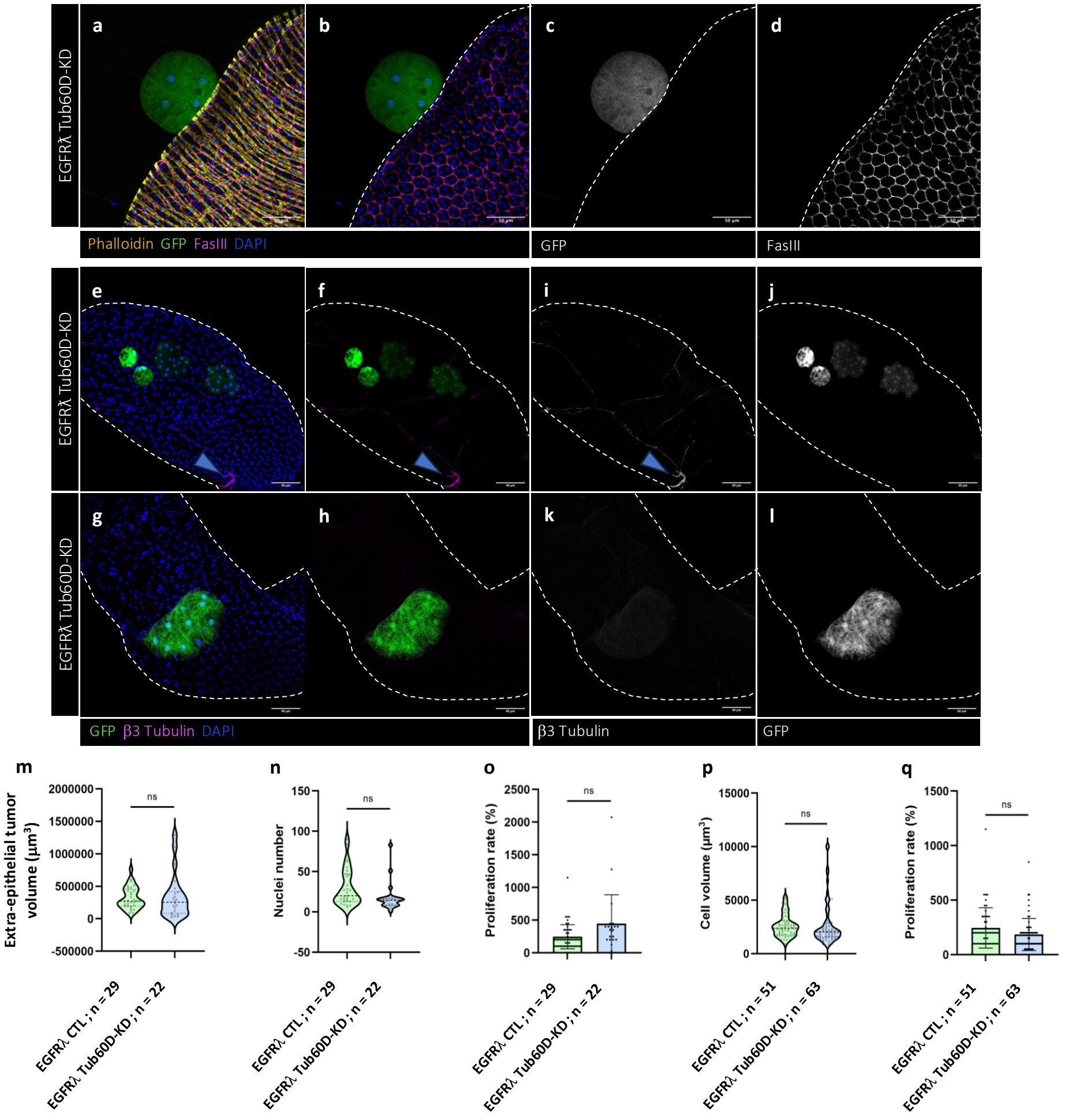

Figure S6- Efficient downregulation of Tub60D has little effect on epithelial tumor cells.
(a-d) Co-expression of Tub60D RNAi does not affect the phenotype of extra-epithelial tumors. (e-l) Downregulation of Tub60D efficiently suppresses the accumulation of β3 Tubulin in clonal cells (e-h) and tumor cells (i-l). Remaining staining can be seen in other cell types such as tracheal cells (blue arrowheads in (e-i). (m-r) Characteristics of the different types of tumor cells co-expressing Tub60D RNAi. (m-q) Extra-epithelial tumors co-expressing Tub60D RNAi display the same size (m), cell number (n) and proliferation rate (o) as EGFRλ CTL tumors. (p-q) Intra-epithelial clones co-expressing Tub60D RNAi are composed of cells of same size (p) and display the same proliferation rate (q) as EGFRλ CTL intra-epithelial clones. Chi^2 test; ns non significant. Representative images in (a-l) from three or more experiments. Scale bars: 50 µM.